T-1243

INVESTIGATION OF DISPLACEMENT STEPS IN A LAYERED HALF-SPACE BY THE FINITE-DIFFERENCE METHOD

By

Hans Leitinger

ProQuest LLC.
789 East Eisenhower Parkway
P.O. Box 1346
Ann Arbor, MI 48106 – 1346

T-1243

A Thesis submitted to the Faculty and the Board of Trustees of the Colorado School of Mines in partial fulfillment of the requirements for the degree of Doctor of Philosophy in Geophysical Engineering.

Signed: J. Hans Leitinger
J. Hans Leitinger

Golden, Colorado

Date: 13 MAY, 1969

Approved: Frank A Hadsell
Frank A. Hadsell
Thesis Advisor

John C. Hollister
Head of Department

Golden, Colorado

Date: 13 MAY, 1969

ABSTRACT

A finite difference solution of the wave equation was applied to investigate displacement steps and associated transients in layered half-spaces[1/]. The prime task was to establish relationships for the attenuation with the distance from a point source of the remnant displacement[2/] of a step-like displacement pulse on the surface of the layered half-spaces.

The homogeneous isotropic half-space, two-layer models, and three-layer models were investigated. For the two-layer model, three different model conditions are presented. They are for three different rigidities in the half-space, with all other model parameters constant. For the three-layer model, again three different model conditions are presented. They are for three different rigidities in the second layer, with all other model parameters constant.

1/ An n-layered half-space or n-layer model is defined as a semi-infinite medium of n-1 parallel, homogeneous, isotropic layers of finite thickness, and an n-th layer of infinite thickness.

2/ The remnant of a step-like displacement pulse is defined as the displacement remaining at any point of the layered half-space, after the transient displacements have died out.

For the one-layer model, the remnant displacement had an amplitude to distance relationship of R^{-2} as predicted by other theories. Two-layer models with a small rigidity contrast between the first and the second layer show approximately the same behavior. As the rigidity in the second layer is decreased, the attenuation of the remnant displacement still shows approximately the same behavior as the one-layer model near the source; however, from a distance of approximately three to four source depths on, the attenuation decreases with distance. For a rigidity ratio of $\mu_2/\mu_1 = 0.211$, a ratio of compressional wave speeds of $v_{c2}/v_{c1} = 4/3$, and a density ratio of $\rho_2/\rho_1 = 3/2$ the total amplitude of the remnant displacement is related to the distance from the point source as $R^{-1.1}$ at an epicentral distance of eight source depths.

As the rigidity of the second layer is lowered, the three-layer model shows a small decrease in attenuation of the remnant displacement. Quantitative predictions of the relationship of amplitude to distance from the point source were not made for the three-layer model. Rayleigh waves[1/], induced in the

---

1/ Rayleigh waves are defined according to Ewing, et al (1957) as vertically polarized surface waves with a retrograde elliptical particle motion. They attenuate exponentially with the distance from the surface and propagate at a speed which is frequency dependent in a layered half-space.

three-layer model, mask the amplitude of the remnant displacement at the range of distances from the source investigated. Thus, with a computer of the size used for this investigation, a quantitative prediction of the attenuation for the present model conditions by this method was not possible.

For the one-layer model at an epicentral distance of eight source depths, approximately 16 percent of the amplitude of the horizontal remnant displacement was present after the compressional wave transient. The remaining 84 percent was added during the Rayleigh wave transient. For the multi-layer models such a quantitative statement cannot be made. The synthetic seismograms indicate, however, that most of the remnant displacement arrives with the Rayleigh wave train.

A CDC 6400 computer with a central memory of 65,536 60-bit words was used to carry out the investigation. The computation time for a model of 11,500 grid points is approximately forty minutes for 500 time cycles.

ACKNOWLEDGMENTS

I should like to express my sincere gratitude to the Mobil Research and Development Corporation for its financial support during my graduate studies and for the opportunity to do my thesis research as a member of the Geophysics Group of the Field Research Laboratory with unlimited use of the computer facility. Only this generous support made the present research project possible.

To Prof. John C. Hollister goes my deepest appreciation for inducing me to do graduate work in Geophysics and for serving on my doctoral committee. I am grateful to Prof. Frank A. Hadsell for acting as advisor on this research project, to Mr. Frank J. McDonal, Mobil Oil Corporation,for acting as off-campus advisor and to Dr. Robert J. Watson, Mobil Oil Corporation,for suggesting the research topic.

I am also indebted to Mr. William C. Gray, Mobil Oil Corporation, for his counsel in developing the computer programs, to Dr. William H. Ruehle, Mobil Oil Corporation, for many stimulating discussions, and to Mrs. Sarah Brister, for her patience in preparing the thesis.

CONTENTS

ILLUSTRATIONS

LIST OF SYMBOLS

A	Horizontal displacement
AR	Reflected horizontal displacement inside the control zone
AS	Horizontal displacement due to the point source in an infinite medium
B	Vertical displacement
BR	Reflected vertical displacement inside the control zone
BS	Vertical displacement due to the point source in an infinite medium
D	Source depth
R	Distance from the source point to a point in the displacement field
r	Radial coordinate of a point in the displacement field
t	Time
v	Wave speed
z	Vertical coordinate of a point in the displacement field
FD2LA	Fortran program for two-layer model
FD3LBA	Fortran program for three-layer model

Δ	Time constant of source potential
Δr	Radial space increment
Δz	Vertical space increment
$\Phi_o(t)$	Source potential
λ, μ	Lamé constants
ρ	Density

Subscripts

c	Compressional
m	Radial index of a point in the displacement field
n	Vertical index of a point in the displacement field
p	Time index of displacements
r	Radial
s	Shear
z	Vertical

Superscripts

1	Medium 1
2	Medium 2

INTRODUCTION

Permanent adjustments in the strain field of the earth after earthquakes have been reported by several investigators. Wideman and Major (1967), in their quantitative study of these permanent adjustments or strain steps, arrived at a strain amplitude dependence upon distance from the source of $R^{-3/2}$. Their study was based on a correlation of earthquake magnitudes and observed strain. Major (1968) later confirmed this relationship from observations of strain data at two distances from an underground nuclear explosion. Wideman and Major (1967) further report strain step speeds of 3.0 ± 0.3 km/sec for a continental path and 3.6 km/sec for an oceanic path.

For a homogeneous isotropic half-space, the theory of static elasticity predicts an amplitude to distance dependence for strain steps of R^{-3}. A similar relationship is to be expected for a layered half-space in which the individual layers have approximately the same rigidity. Hadsell and Major (1968) suggested that an abnormally low rigidity in the lower crust or upper mantle may be the reason for the observed amplitude to distance relationship.

In this research an attempt was made to explain this relationship by mathematically modelling the earth's crust and

upper mantle. The finite-difference solution of the wave equation for the three-dimensional, axially symmetric case was used to do the modelling.

Alterman and Karal (1968), pioneers in the finite-difference approach to the solution of the wave equation, presented the solutions in a homogeneous isotropic half-space and a single layer on a half-space. They also presented a comparison of the finite-difference method to an exact ray method for the same model of a layered half-space to establish the accuracy of the finite-difference approach.

Following the derivations of the Alterman-Karal paper, computer programs were implemented for four cases, three of which are treated in this paper. The four cases are as follows:

(1) the homogeneous isotropic half-space

(2) the two-layer model with the Lamé constants in the upper layer higher than those in the lower layer.

(3) the two-layer model with the Lamé constants in the upper layer lower than those in the lower layer.

(4) the two-layer model with $\mu_1 > \mu_2$ and $\rho_1 v_{c1}^2 < \rho_2 v_{c2}^2$. These conditions were incompatible with the Alterman-Karal algorithms; thus a special set of boundary condition algorithms was designed for this study.

A point source with a step-like displacement potential was used to test the programs (see Figure 2). A source potential generates a displacement pulse consisting of a near-field and a far-field term. For the investigation of the displacement steps in a layered medium, only the near-field term of the displacement pulse was used. This term has the same time dependence as the source potential.

The displacement step was investigated for the one-layer model and for a two-layer model with varying elastic conditions in the second layer. Shear-wave speeds as low as 1 km/sec in the second layer (mantle) were employed in this investigation. These elastic conditions do not fit the actual conditions in the earth very well, unless a rather unlikely rheological behavior of the mantle is assumed.

On the basis of Rayleigh-wave dispersion, Gutenberg (1932) and others have shown that the shear-wave speed in the upper mantle is approximately 4.5 km/sec for 7- to 70-sec periods. Haskell (1953) calculated Rayleigh-wave dispersion curves for various models of the crust and upper mantle for the same range of periods. He shows that a three-layer model can have almost the same dispersion curve as a two-layer model, if the first and the third layer have the same elastic conditions as the first and second layer of the two-layer model. Either one of these models would fit the observed Rayleigh-wave dispersion equally

well. The negligible effect of the second layer of a three-layer model on the Rayleigh-wave dispersion suggested the investigation of a three-layer model, in which the rigidity of the second layer could be lowered abnormally without disturbing the proper Rayleigh-wave dispersion.

Two cases of three-layer models were implemented for numerical calculations. In the first case, the Lamé constants of the second layer are lower than those of the first and the third layer. The second case is for the conditions $\rho_1 v_{c1}^2 < \rho_2 v_{c2}^2 \leq \rho_3 v_{c3}^2$ and $\mu_1 > \mu_2 < \mu_3$.

STATEMENT OF TWO-LAYER PROBLEM AND FORMULATION OF ALGORITHMS

The problem is to determine the motion of any point on or within a homogeneous isotropic layer which is in welded contact with a homogeneous isotropic half-space. An isotropic displacement pulse is assumed to originate at a point source in the layer. Figure 1 shows the geometry and elastic parameters

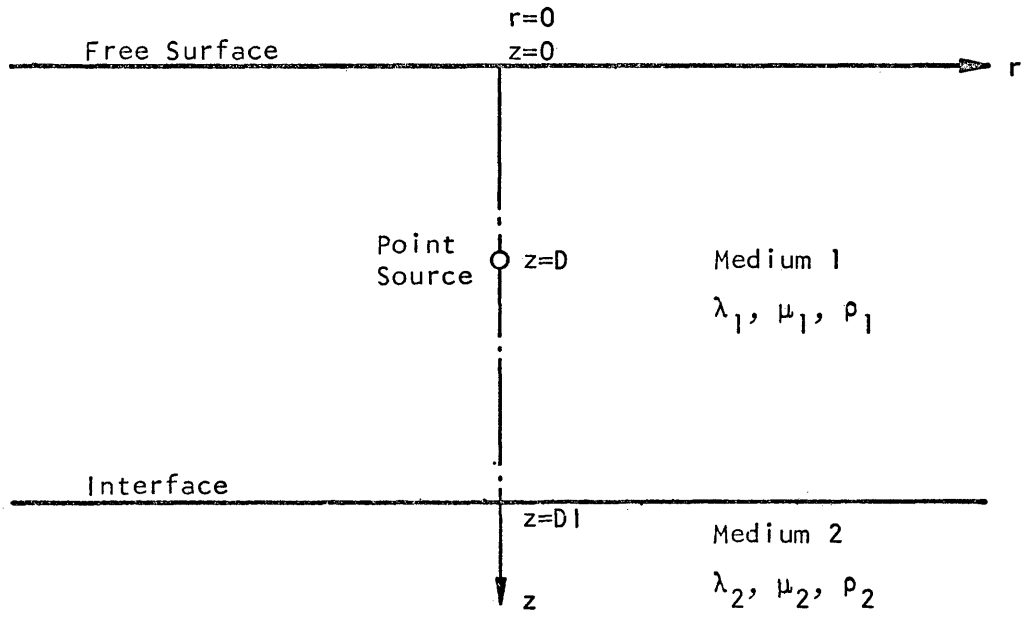

FIGURE 1. Geometrical Configuration of the Model.

for this model. Because the model has axial symmetry, cylindrical coordinates are used. The z-axis passes through the source and is positive downward.

The developement of the algorithms for the various models was based on the mathematical derivations given by Alterman and Karal (1968). [The Alterman-Karal paper contains a number of printing errors whose corrections are given by Alterman-Karal (1969)]. The finite-difference equations for the boundary conditions of model (4) differ somewhat from the Alterman-Karal developements, and are shown in the next section.

The source function used by Alterman and Karal was applied here to test the algorithms by duplicating a number of seismograms shown by these authors. For the investigation of the displacement steps in layered media, only the near-field term of the source pulse was used. It has a step-like time dependence (Fig. 2) like the source potential. The use of the near-field term avoided unnecessary interference of strong transient waves, which are of no immediate interest to the present research.

Algorithm for Model (4) -- Model (4) is the case of a layer on a half-space with $\rho_1 v_{c1}^2 < \rho_2 v_{c2}^2$ and $\mu_1 > \mu_2$. This model condition is of special interest in the present research. Either one of the two algorithms for the two-layer model introduced by Alterman and Karal would be subject to instability under these conditions. The instability is induced in the calculation of the boundary conditions whenever either one of the ratios μ_1/μ_2 and $\rho_1 v_{c1}^2/\rho_2 v_{c2}^2$ becomes larger than one. To avoid this condition, equations (27) and (29) of the

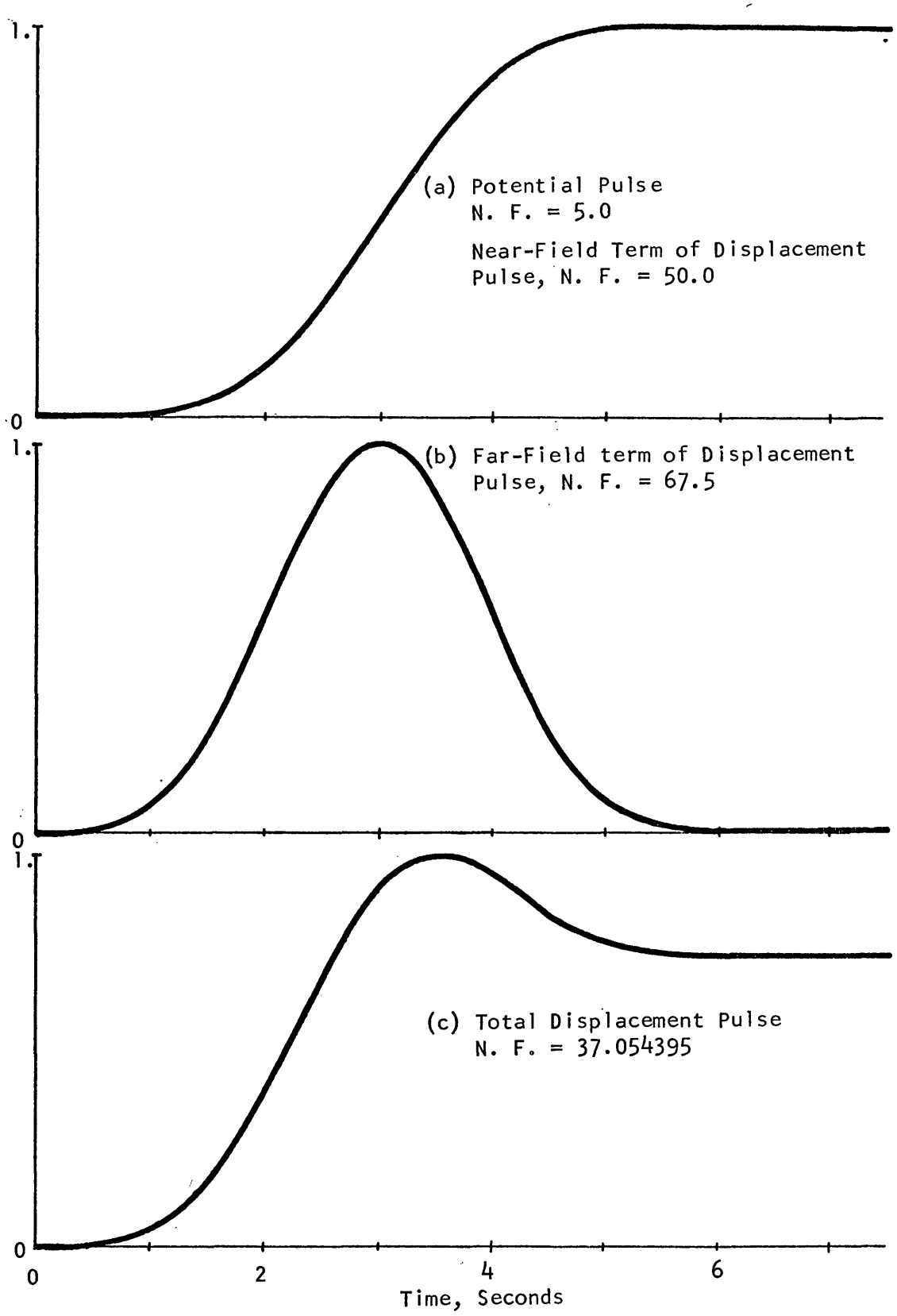

FIGURE 2. Normalized Potential Pulse and Near-Field Term (a) of, Far-Field Term (b) of, and Total Displacement Pulse (c) from Point Source. Distance from Source 10 km, v_c = 6 km/sec, Pulse length = 6 sec. N. F. = Normalizing Factor.

Alterman-Karal paper are used to maintain the continuity of shear stresses, and equations (32) and (34) to maintain the continuity of normal stresses across the interface. The use of this set of equations at the interface boundary requires the ficticious extension of the layer into the half-space, as well as the ficticious extension of the half-space into the layer (Figure 3). The z-index of the interface

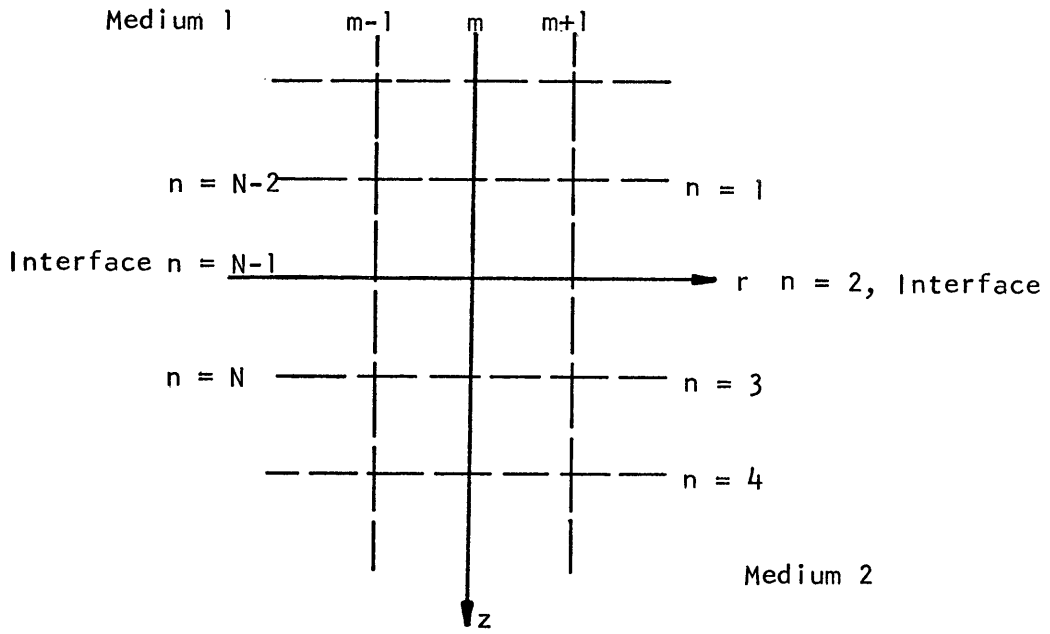

FIGURE 3. Grid Arrangement at the Interface for Model 4.

in the layer is N-1; that of the last grid line of the layer is N. The z-index of the first grid line in the half-space is 1; that of the interface is 2.

Because the two stress boundary conditions are applied in two different media, one of the displacements is missing on the ficticious lines on either side of the interface. There are no equations for $B^1_{m,N,p+1}$ and $A^2_{m,1,p+1}$. To carry the computation of the displacements by the equations of motion to the interface n = N-1 in medium 1, one-sided backward derivatives in z were used for $\partial^2 B/\partial r \partial z$ in equation (3) of the Alterman-Karal paper for the last step upon approaching the interface in z-direction. Equally, to start the computation of displacements by the equations of motion at the interface n = 2, one-sided forward derivatives in z were used for $\partial A/\partial z$ and $\partial^2 A/\partial r \partial z$ in equation (4) of the Alterman-Karal paper for the first step in z-direction in medium 2. Simple two-point finite-difference approximations were used for the first derivatives with respect to z. Thus, the displacements at the interface for the present case are given by

$$A^1_{m,N-1,p+1} = 2A^1_{m,N-1,p} - A^1_{m,N-1,p-1} + (v_{c1}\Delta t/\Delta r)^2(A^1_{m+1,N-1,p} - 2A^1_{m,N-1,p} + A^1_{m-1,N-1,p}) + \frac{1}{2}(v_{c1}\Delta t/\Delta r)^2(1/m) \times (A^1_{m+1,N-1,p} - A^1_{m-1,N-1,p}) - (v_{c1}\Delta t/\Delta r)^2(1/m^2)A^1_{m,N-1,p} + \frac{1}{2}(v_{c1}\Delta t/\Delta r)^2(\Delta r/\Delta z)[1-(v_{s1}/v_{c1})^2](B^1_{m+1,N-1,p} - B^1_{m+1,N-2,p} - B^1_{m-1,N-1,p} + B^1_{m-1,N-2,p}) +$$

$$(v_{c1}\Delta t/\Delta r)^2(\Delta r/\Delta z)^2(v_{s1}/v_{c1})^2(A^1_{m,N,p} - 2A^1_{m,N-1,p} +$$

$$A^1_{m,N-2,p}), \qquad (1)$$

$$A^2_{m,2,p+1} = A^1_{m,N-1,p+1}, \qquad (2)$$

$$B^2_{m,2,p+1} = 2B^2_{m,2,p} - B^2_{m,2,p-1} + (v_{c2}\Delta t/\Delta r)^2(\Delta r/\Delta z)^2(B^2_{m,3,p} -$$

$$2B^2_{m,2,p} + B^2_{m,1,p}) + (v_{c2}\Delta t/\Delta r)^2(\Delta r/\Delta z)(1/m)$$

$$x[1 - (v_{s2}/v_{c2})^2](A^2_{m,3,p} - A^2_{m,2,p}) + \tfrac{1}{2}(v_{c2}\Delta t/\Delta r)^2$$

$$x[1 - (v_{s2}/v_{c2})^2](\Delta r/\Delta z)(A^2_{m+1,3,p} - A^2_{m+1,2,p} -$$

$$A^2_{m-1,3,p} + A^2_{m-1,2,p}) + (v_{c2}\Delta t/\Delta r)^2(v_{s2}/v_{c2})^2(B^2_{m+1,2,p}$$

$$- 2B^2_{m,2,p} + B^2_{m-1,2,p}) + \tfrac{1}{2}(v_{c2}\Delta t/\Delta r)^2(v_{s2}/v_{c2})^2(1/m)$$

$$x(B^2_{m+1,2,p} - B^2_{m-1,2,p}), \qquad (3)$$

$$B^1_{m,N-1,p+1} = B^2_{m,2,p+1}, \qquad (4)$$

for $m > 0$ and for the z-axis ($m = 0$),

$$A^1_{0,N-1,p+1} = A^2_{0,2,p+1} = 0 \qquad (5)$$

$$B^2_{0,2,p+1} = 2B^2_{0,2,p} - B^2_{0,2,p-1} + (v_{c2}\Delta t/\Delta r)^2(\Delta r/\Delta z)^2(B^2_{0,3,p} -$$

$$2B^2_{0,2,p} + B^2_{0,1,p}) + 2(v_{c2}\Delta t/\Delta r)^2(\Delta r/\Delta z)[1 - (v_{s2}/v_{c2})^2]$$

$$x(A^2_{1,3,p} - A^2_{1,2,p}) + 4(v_{c2}\Delta t/\Delta r)^2(v_{s2}/v_{c2})^2(B^2_{1,2,p} -$$

$$B^2_{0,2,p}), \text{ and} \qquad (6)$$

$$B^1_{0,N-1,p+1} = B^2_{0,2,p+1}. \qquad (7)$$

For all other points of media 1 and 2 the equations of motion (15), (16), (17), and (19) of the Alterman-Karal paper may be used to propagate an elastic disturbance.

Source Boundary Conditions -- Alterman and Karal (1968) gave an elegant treatment for handling the point compressional source. This method was adopted for the present research. Figure 6 of the above reference shows the geometry of a source region surrounding the point source and shows the relationship between three components of the horizontal and vertical displacements. For the horizontal displacement, these components are A, the total horizontal displacement outside of the source region; AS, the horizontal displacement component in the layer containing the source which is contributed by the source; AR, the horizontal displacement component in the layer containing the source which is contributed by reflections from interface boundaries with other media. The same components exist for the vertical displacement. Because we are dealing with a linear system, they are related by

$$\begin{aligned} A &= AS + AR, \text{ and} \\ B &= BS + BR., \end{aligned} \qquad (8)$$

Now it is assumed that the displacement field A and B is known for time $t = (p-1)\Delta t$ and $t = p\Delta t$ for all points of the inner- and outer-source-region boundary and for all points outside of the source region. The displacement field AR and BR is also assumed to be known inside the source region and on its boundaries for these two instances in time. From Figure 3 of the Alterman-Karal paper, the displacement field A and B can now be computed for the time $t = (p+1)\Delta t$ for all points outside the source region and on the outer-source-region boundary, using equations(15) and (16) of the same reference. The calculation stencil for this displacement field is shown in Figure 4. Similarly, the displacement field AR and BR can now be computed for $t = (p+1)\Delta t$ for all points inside the source region excluding the outer region boundary, using again the finite difference equations (15) and (16). The calculation stencil for this process is shown in Figure 5. Physically, these adjustment processes of the displacements go on at the same time. Thus it is immaterial in which sequence they are arranged in the algorithm.

To complete the displacement fields for the time $t = (p+1)\Delta t$, A and B must be calculated for the inner boundary of the source region and AR and BR for the outer boundary of the source region. A_{p+1} and B_{p+1} are determined by calculating AS_{p+1} and BS_{p+1} for all points of the inner- and outer-source-region

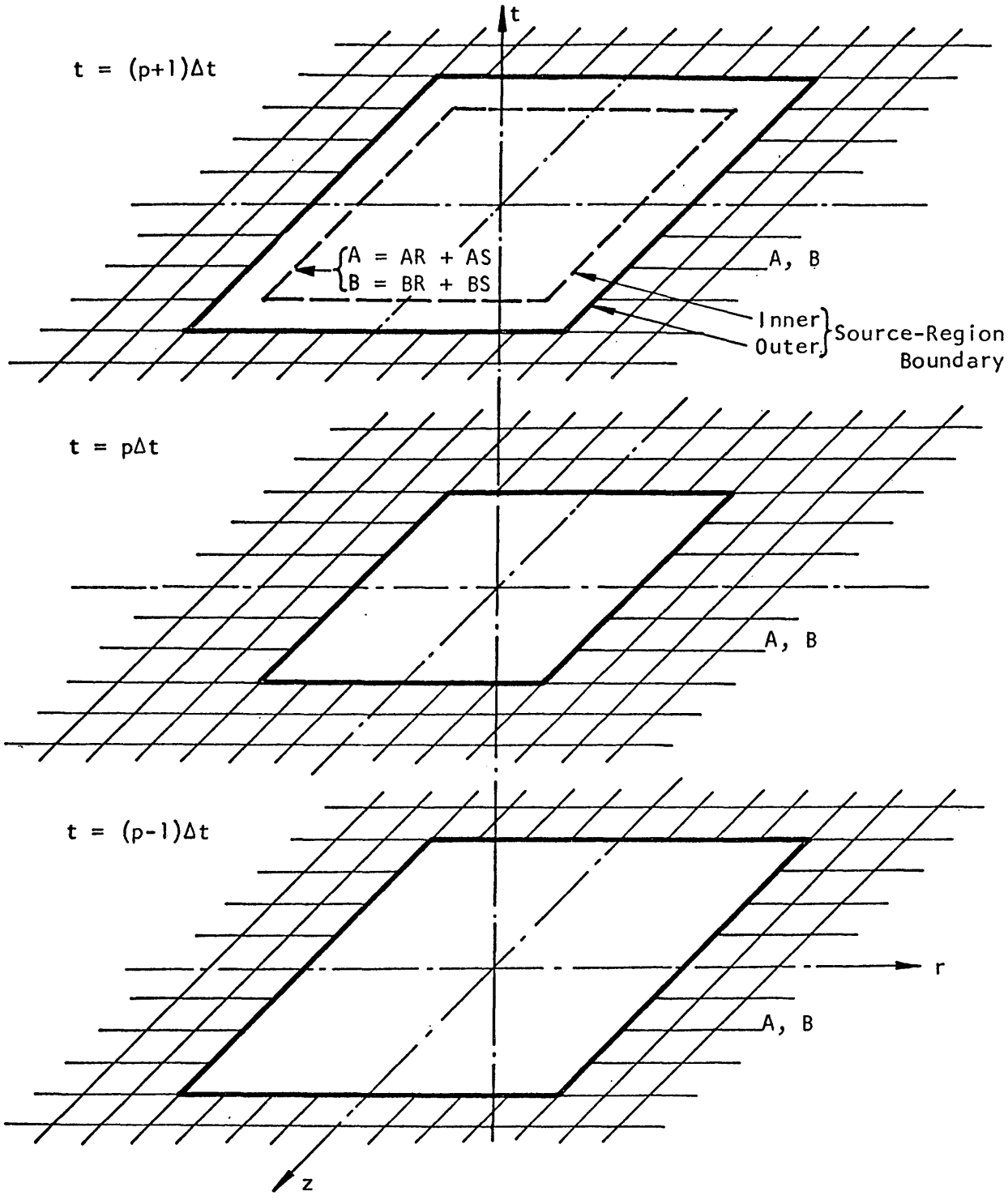

FIGURE 4. Calculation Stencil for A and B by Finite Difference-Equations Outside of Source Region and on Outer-Source-Region Boundary, and by Superposition on Inner-Source-Region Boundary.

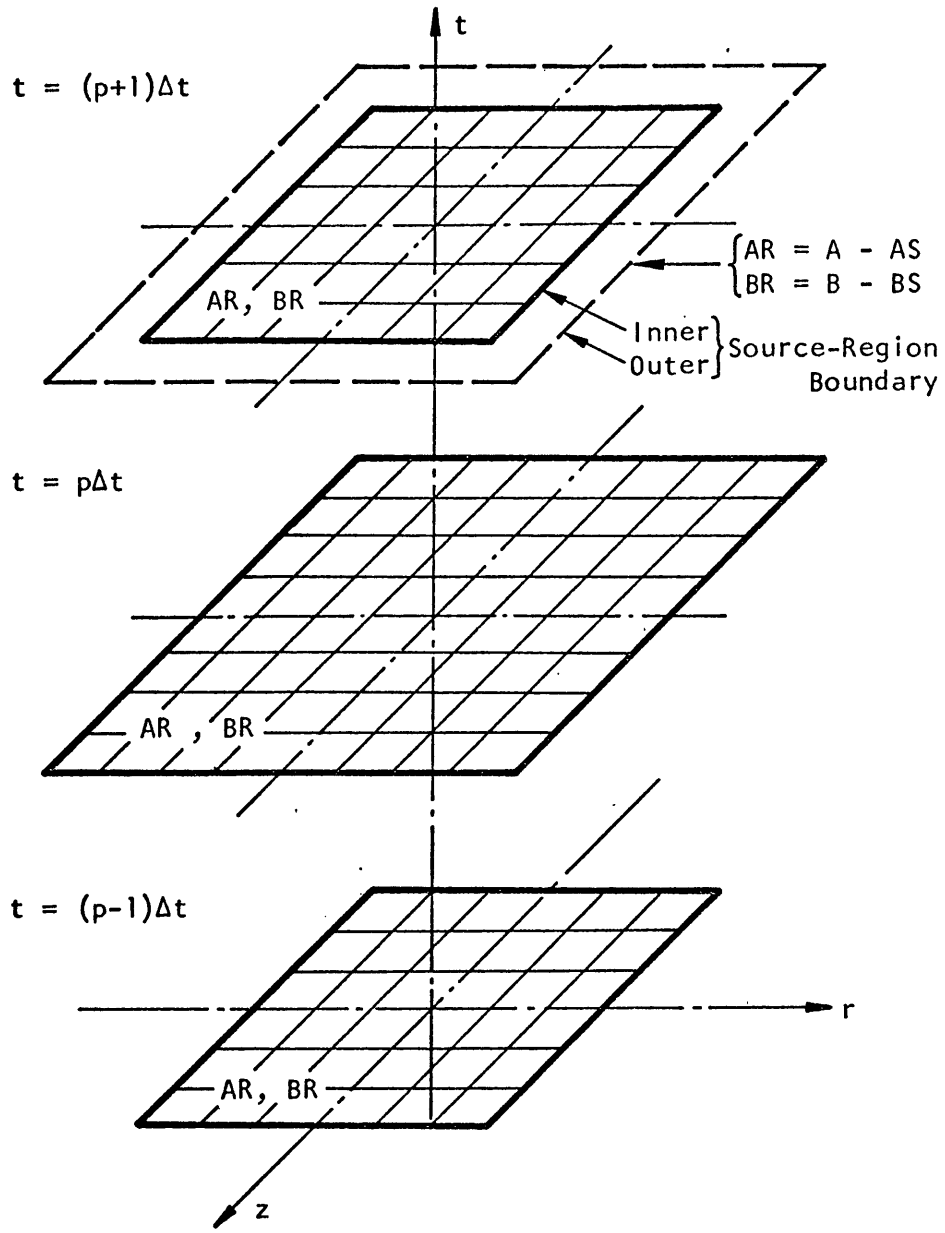

FIGURE 5. Calculation Stencil for AR and BR by Finite-Difference Equations Inside the Source Region and on Inner-Source-Region Boundary, and by Superposition on Outer-Source-Region Boundary.

boundary with the time-distance relationship for the source pulse. With AR_{p+1} and BR_{p+1} known on the inner-source-region

boundary, A_{p+1} and B_{p+1} can be calculated for all points of this boundary using equation (8). Similarly, since A_{p+1} and B_{p+1} are known for all points of the outer-source-region boundary, AR_{p+1} and BR_{p+1} can be calculated using equations (8). These processes are also indicated in Figures 4 and 5.

Now the complete displacement field is known for p+1, and the process may be repeated for the next instant in time.

Initiation of Computation -- At the time t = 0, all points of the medium have zero displacement. A compressional pulse emanating from the point source propagates as in an infinite medium until it reaches the nearest interface boundary with another medium. Therefore, the displacement field is calculated for the time of the first arrival of the compressional pulse at the nearest interface t = TFA and for t = TFA + Δt, using the time-distance relationship for the source displacements

$$A = \partial\Phi_o/\partial r$$
$$B = \partial\Phi_o/\partial z. \qquad (9)$$

The stability criterion requires that $v_c\Delta t < \Delta z$. Thus at the time t = TFA + Δt, the reflected P-wave front has not yet returned to the grid line next to the interface. The displacements at this grid line are, therefore, purely determined by the source pulse at this instant of time. Calculation

of the boundary conditions for t = TFA and TFA + Δt completes the initial displacement field.

With the displacement field known for two successive instants in time, the finite difference computation may now be initiated. First, the equations of motion (15), (16), (17), and (19) of the Alterman-Karal paper are used to compute the displacement field within the layer, the source region, and the half-space, excluding the boundaries. The displacements on the boundary grid lines are then computed using the respective equations for the boundary conditions. The displacements at the receiver locations of interest are now stored and the computational cycle is completed.

Figure 3 of the Alterman-Karal paper indicates that to compute A_{p+1} and B_{p+1} at a point, A_{p-1} and B_{p-1}, respectively, must be known at this point. In addition A_p and B_p must be known at the point and all points surrounding it. Thus, once A_{p+1} is computed, A_{p-1} is no more required and A_{p+1} is stored in its location. Similarly, B_{p+1} is stored in the location of B_{p-1}. This procedure allows larger displacement arrays.

DISCUSSION OF MODELS

Fortran programs, implemented for the various models mentioned previously, were tested against the results given by Alterman and Karal (1968). Because the size of the source region is not given in the Alterman-Karal paper, a number of test runs had to be made to establish the optimum size for the source region. A radius and half-height of seven space increments produced the same seismograms.

In these test calculations, the fulfillment of the stability criterion is not the only requirement to be observed to obtain satisfactory seismograms. In some instances small-amplitude, short-period oscillations around the true displacement values were observed, although the computation was stable. This effect occured when short pulse lengths were used. Smaller time and space increments eliminated this phenomenon, indicating that it was a sampling effect.

In the following discussion, dimensionless length and time parameters are used. The dimensionless length is defined as the ratio of the length to the source depth. Thus, the dimensionless radial increment is $\Delta r/D$. The dimensionless time is defined as the ratio of the product of time and shear-wave speed in medium 1 to the source depth tv_{s1}/D. The dimesionless length of the source pulse is, therefore, $4\Delta v_{s1}/D$.

One-Layer Model -- Figure 6 shows three synthetic seismograms computed with Fortran program FDH for a one-layer model with a dimensionless pulse length of 0.8 and $v_{c1} = \sqrt{3}\, v_{s1}$. This figure corresponds to Figure 10 of the Alterman-Karal paper. With dimensionless space and time increments of 0.1 and 0.03, respectively, Gibbs oscillations were superimposed on the Rayleigh waves as mentioned above. When the increments were decreased to 0.05 and 0.015, respectively, the Gibbs oscillations disappeared. The agreement of Figure 6 and Figure 10 of the Alterman-Karal paper is satisfactory within the measuring accuracy. Both are plotted for the same variables, i. e., the product of the displacements and the square of the distance from source to receiver against the dimensionless time. The computational parameters were chosen to give the same numerical displacements cited in the Alterman-Karal paper.

Figure 7 shows the attenuation of the horizontal component of the Rayleigh wave with depth in a half-space model. It corresponds to Figure 13 of the Alterman-Karal paper. The agreement is excellent within the measuring accuracy of the graphs in Figure 13.

The synthetic seismograms of the present report are shorter than those in the Alterman-Karal paper, a condition caused by the smaller memory of the computer on which the present computations were made.

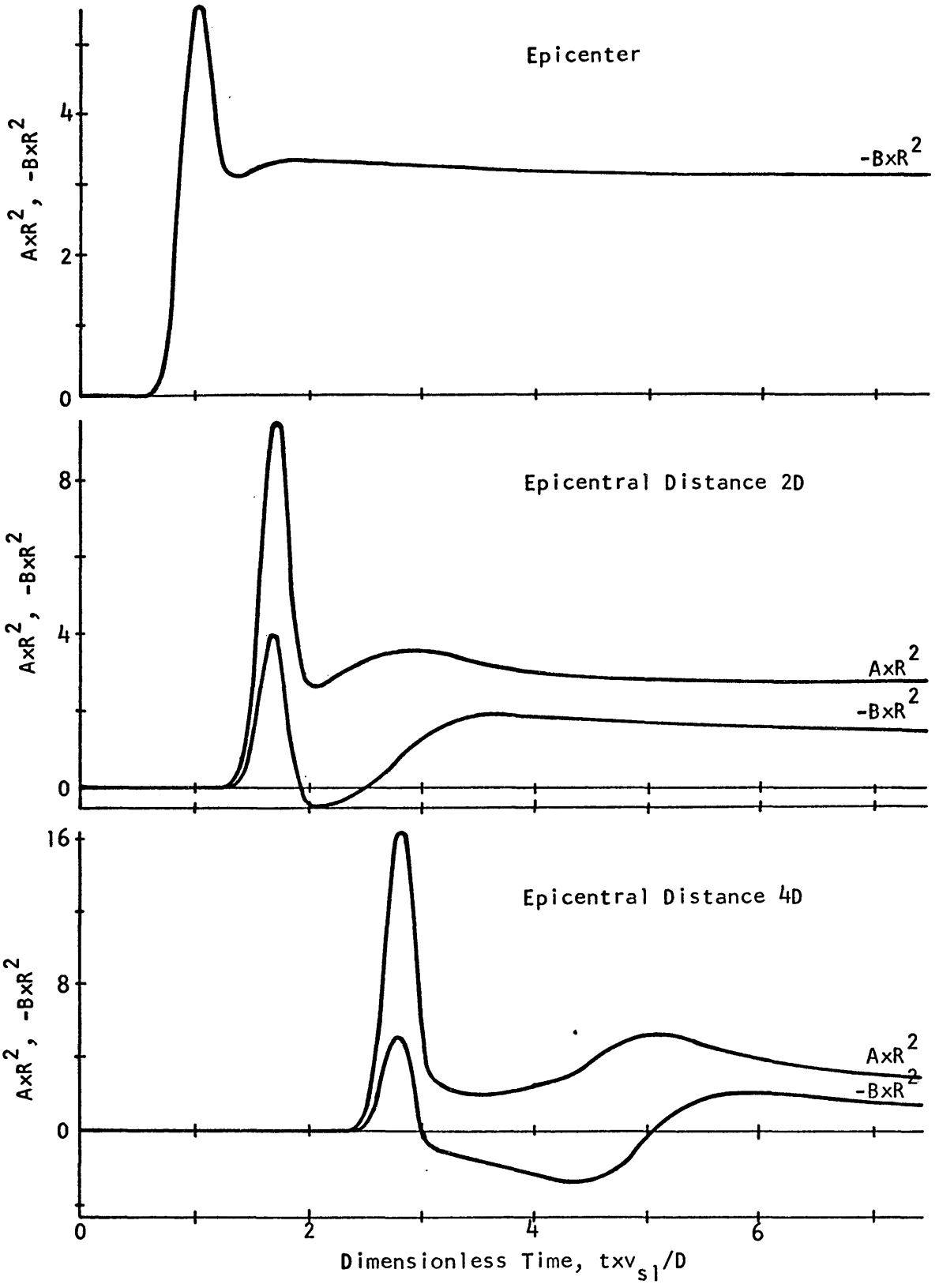

FIGURE 6. Horizontal and Vertical Displacement on the Surface of a Half-Space of $v_{c1}=\sqrt{3}xv_{s1}$, due to a Point Source of Pulse Length 0.8, located at Depth D.

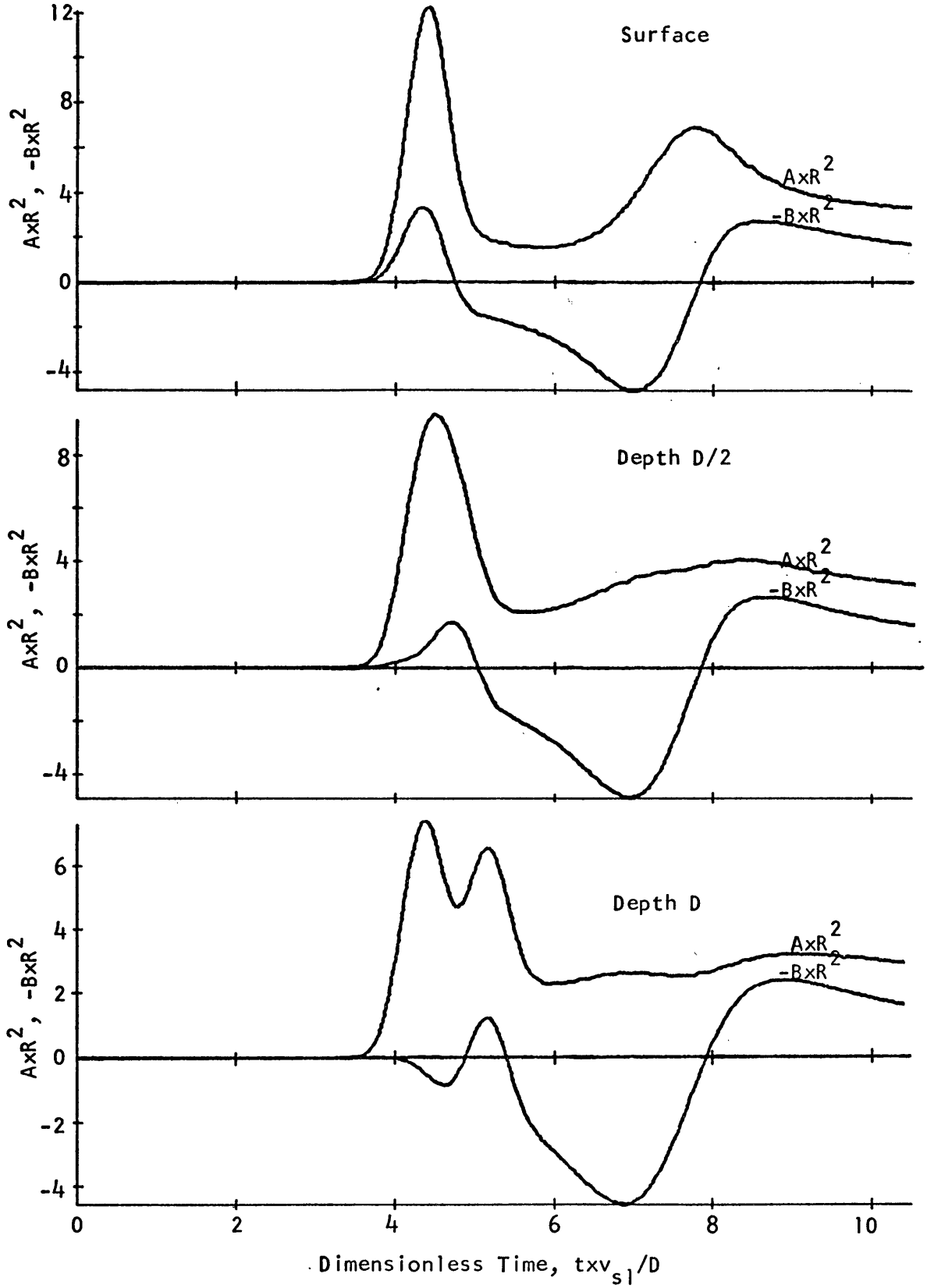

FIGURE 7. Horizontal and Vertical Displacement on and below the Surface of a Half-Space of $v_{c1}=\sqrt{3}xv_{s1}$, due to a Point Source of Pulse Length 1.6. Epicentral Distance of Receivers = 6D.

Two-Layer Models -- Only one case -- case 3 of page 2 -- of the two-layer model has been treated by Alterman and Karal.

Case 1: For this case the Lamé constants of the layer are larger than those of the half-space. Because no comparison exists for this case in the literature, the Fortran program FD2LB was tested by setting the Lamé constants in the half-space equal to zero. If the source is arranged in the center of the layer, the model is a symmetrical slab; seismograms at points opposite to each other on both surfaces will have to be equal with the vertical displacements opposite in direction. The last statement is true only for the exact solution. This can be noted when equations (27) and (28) of the Alterman-Karal paper are written for $\mu_2 = 0$, $\rho_2 = 0$, and $v_{c2} = 0$ and compared with the surface boundary conditions (21) and (22). They are not exactly the same, and thus, the resulting seismograms will be very similar but not the same for two opposite points on the surface. The difference between the two sets of equations is caused by the use of a centered first derivative in z-direction for the surface boundary conditions and a one-sided derivative for the interface boundary conditions.

Figures 8 and 9 show three pairs of synthetic seismograms computed with Fortran program FD2LB for a slab model of $v_{c1}/v_{s1} = 3/2$, $v_{c2}/v_{c1} = v_{s2}/v_{s1} = \rho_2/\rho_1 = 0$ and the source in the center of the slab. The dimensionless length

of the source pulse is 1.6. The receiver pairs are located at the epicenter and at epicentral distances of 2 and 5 source depths. The dimensionless radial and vertical space increments are 0.05. The dimensionless time increment is 0.02. The time origin of these synthetic seismograms is the P-wave arrival time at the epicenter.

The first two graphs of Figure 8 are for the epicenter and the point below the source on the interface, respectively. For easier comparison of the seismograms at two opposite points, the vertival displacements were plotted upside down for points on the interface, i. e., an indicated upward motion is actually down. The wave forms and the time allignment of events match satisfactorily between the two boundaries. There is, however, a small mismatch in amplitudes apparent in the normalizing factors. The maximum displacement at the epicenter is approximately 2.7 percent higher than that at the interface. The last graph of Figure 8 and the first graph of Figure 9 are for an epicentral distance of 2 source depths on the surface and interface, respectively. The last two graphs of Figure 9 are for an epicentral distance of 5 source depths on the surface and interface, respectively. The wave forms and time allignment of events again match satisfactorily for these two pairs of seismograms. The amplitude mismatch here is approximately 1.1 percent. Because the contrast of Lamé constants across the interface for this

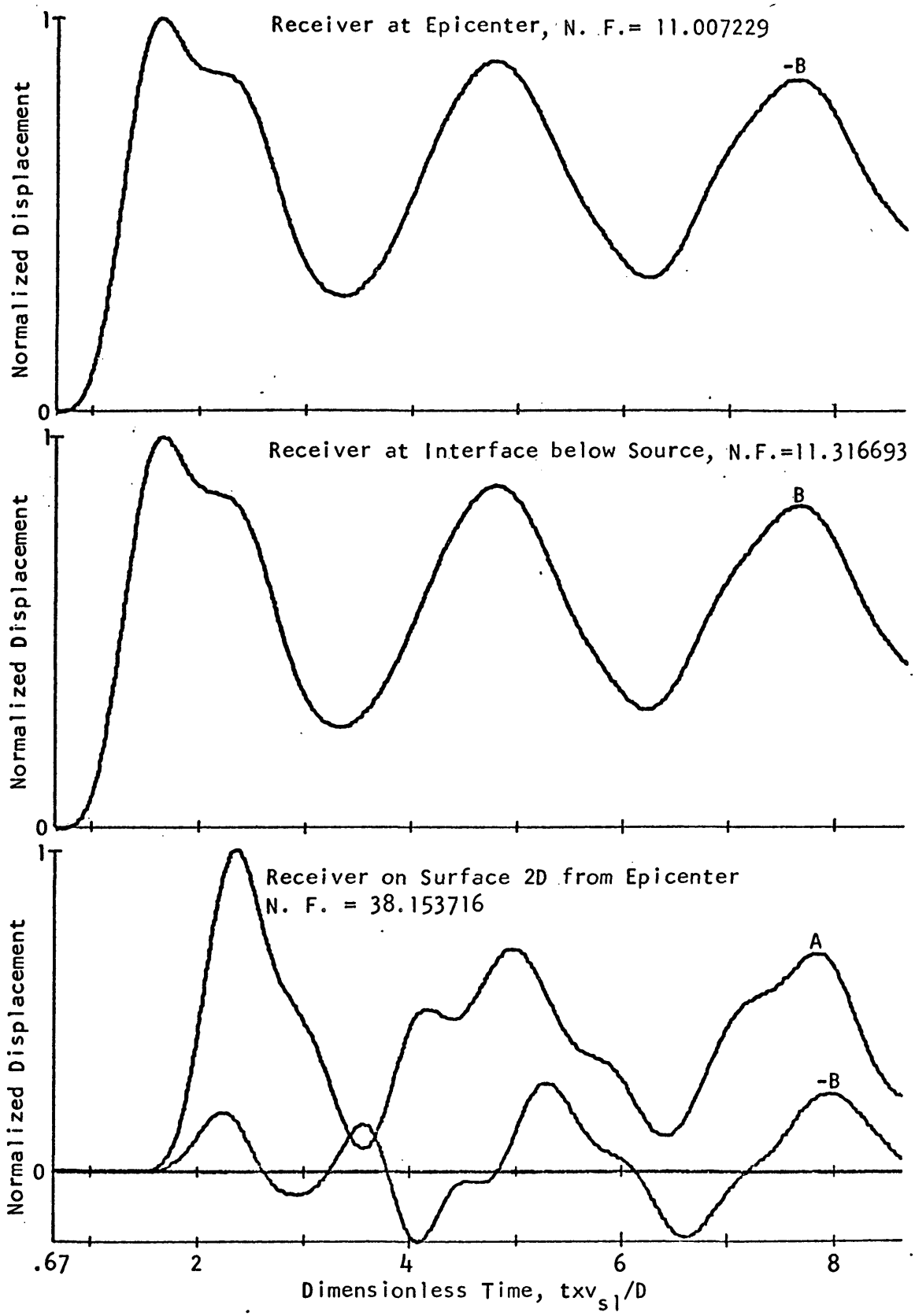

FIGURE 8. Normalized Horizontal and Vertical Displacement on the Surface and Interface of a Layered Half-Space. A Point Source of Pulse Length 1.6 is located at the Center of the Layer.
v_{c1}=6, v_{s1}=4, ρ_1=3, v_{c2}=0, v_{s2}=0, ρ_2=0. N.F.=Normalizing Factor

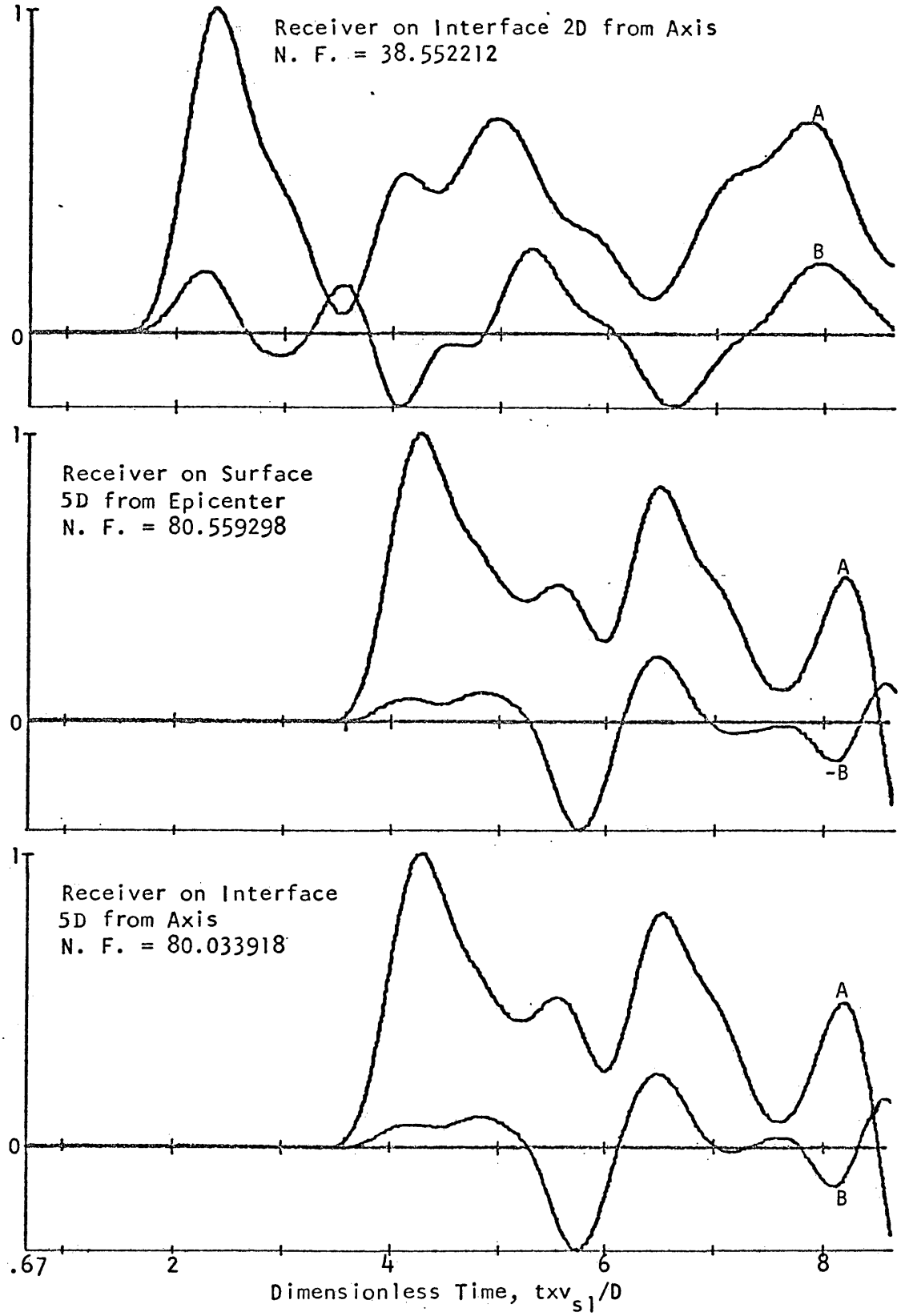

FIGURE 9. Normalized Horizontal and Vertical Displacement on the Surface and Interface of a Layered Half-Space. A Point Source of Pulse Length 1.6 is located at the Center of the Layer. $v_{c1}=6$, $v_{s1}=4$, $\rho_1=3$, $v_{c2}=0$, $v_{s2}=0$, $\rho_2=0$. N.F.=Normalizing Factor

computation is the maximum which can occur for Case 1, it is reasonable to assume that the above discrepancies are the maximum for the present interface boundary conditions. Thus, the scheme may be considered satisfactory.

Case 2: For this case the Lamé constants in the layer are lower than those in the half-space. Fortran program FD2LA was implemented to treat this model.

Figure 10 shows three synthetic seismograms for the present case for $\rho_2 = 1.5\rho_1$, $v_{c2} = 3v_{c1}$, $v_{s2} = 3v_{s1}$ and $\lambda = \mu$. The point source with a dimensionless pulse length of 1.6 is located in the center of the layer. The first two graphs of Figure 10 of this thesis should be compared with Figure 14 of the Alterman-Karal paper; the last graph of Figure 10 should be compared with the first graph of Figure 15 of the Alterman-Karal paper. All seismograms match satisfactorily within measuring accuracy.

Because Alterman and Karal checked their computations against an exact ray method, FD2LA may be considered to treat correctly the model of Case 2.

Case 3: Fortran program FD2LC was designed to treat this case, which requires that $\lambda + 2\mu$ is lower in the layer than in the half-space and the rigidity μ in the layer is higher than that in the half-space.

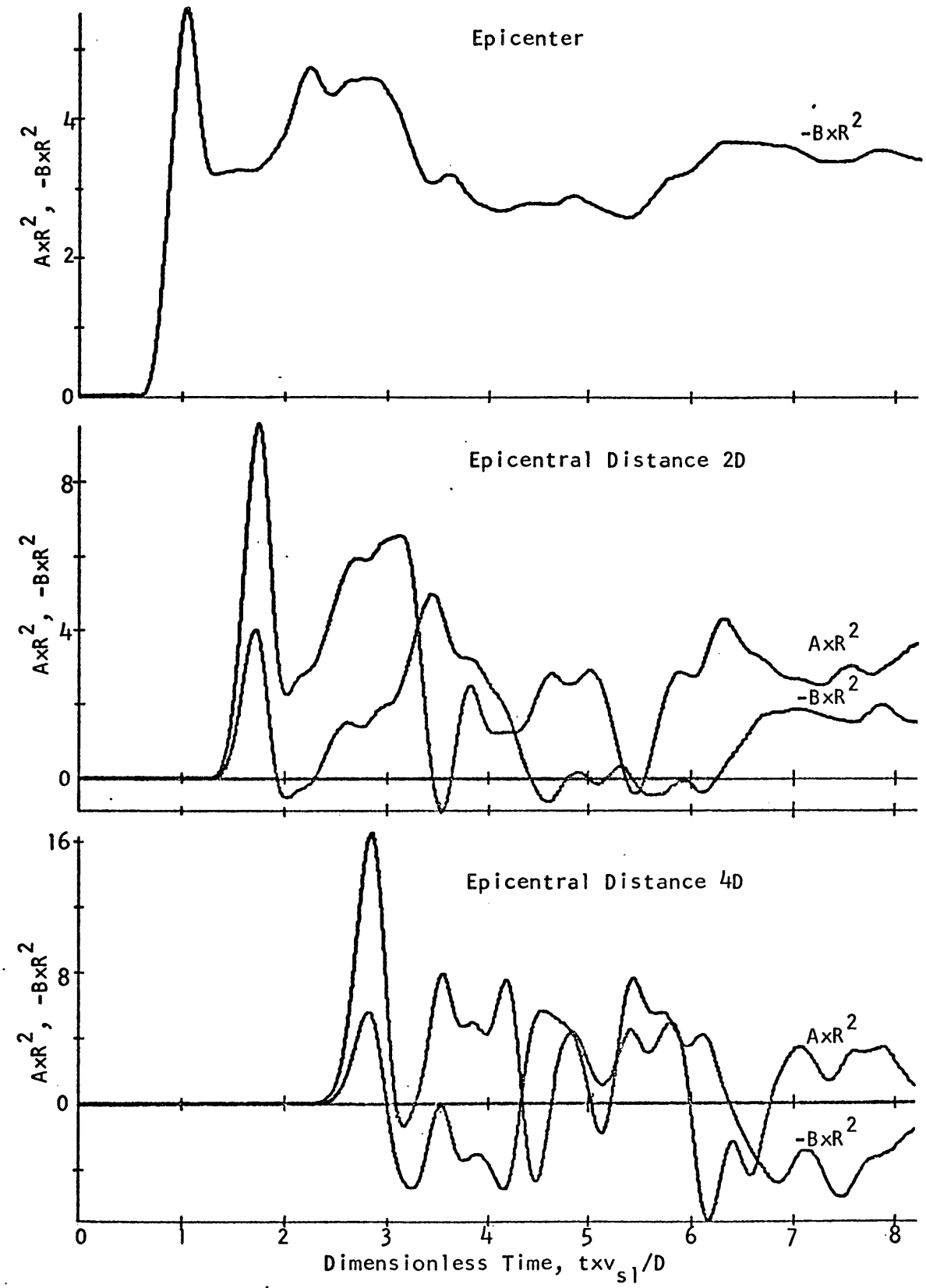

FIGURE 10. Horizontal and Vertical Displacement on the Surface of a Layered Half-Space. A Point Source of Pulse Length 0.8 is located at Depth D. $\rho_2=1.5\rho_1$, $v_{c2}=3v_{c1}$, $v_{s2}=3v_{s1}$, $\lambda=\mu$.

To test the accuracy of FD2LC, model conditions were chosen with $\mu_1 \approx \mu_2$. The same model conditions were then computed with FD2LA and FD2LC. For $\mu_1 \approx \mu_2$ it is to be expected that both approaches are within stable limits for the interface boundary conditions. The model conditions for the test cases are $v_{c1}/v_{c2} = 3/4$, $v_{s1}/v_{s2} = 5/4$, $v_{s1}/v_{c1} = 2/3$, $\rho_1/\rho_2 = 2/3$. The dimensionless radial and vertical space increments are 0.25 and 0.125, respectively, and the dimensionless time increment is 0.0375. A point source with a step-like displacement pulse (see Figure 2)--the near-field term of the complete displacement pulse--with a dimensionless pulse length of 3.0 was chosen for this model.

Figure 11 shows three synthetic seismograms which were computed with FD2LA for receiver locations on the surface at the epicenter and epicentral distances of 4 and 8 source depths.

Figure 12 shows three synthetic seismograms which were computed with FD2LC for the same receiver locations. There is only a slight difference in the wave form of the respective pairs of seismograms. The maximum displacements at the epicenter are the same to 8 digits for both cases, differing by 0.0015 percent at an epicentral distance of 4 source depths and 0.39 percent at an epicentral distance of 8 source depth. Considering that the approach in computing the interface boundary conditions

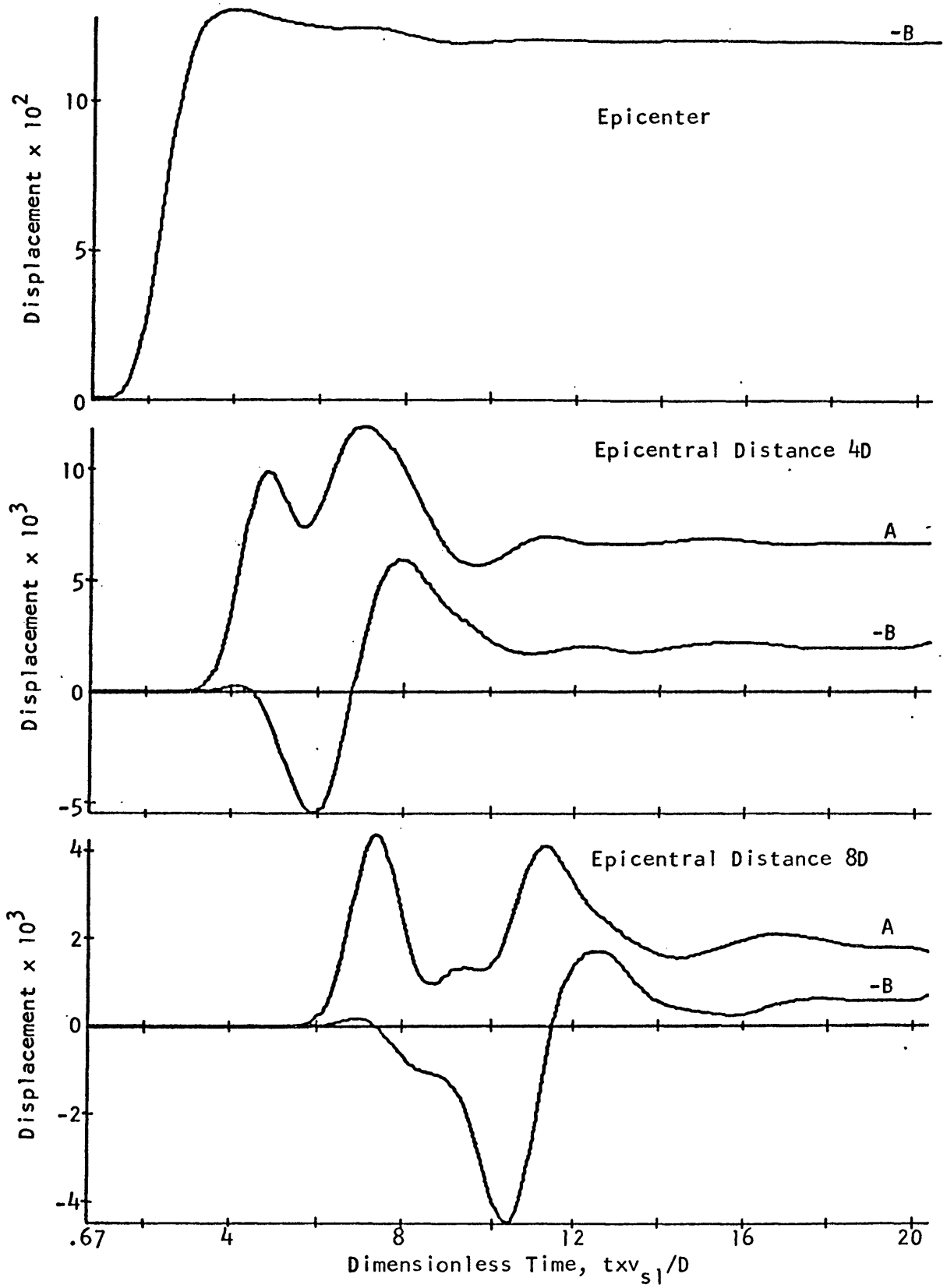

FIGURE 11. Horizontal and Vertical Displacement on the Surface of a Layered Half-Space. A point Source at Depth D has a Step-like Pulse of Length 3. Layer Thickness 4.375D. Computed with FD2LA. $v_{c1}/v_{c2}=3/4$, $v_{s1}/v_{s2}=5/4$, $v_{s1}/v_{c1}=2/3$, $\rho_1/\rho_2=2/3$.

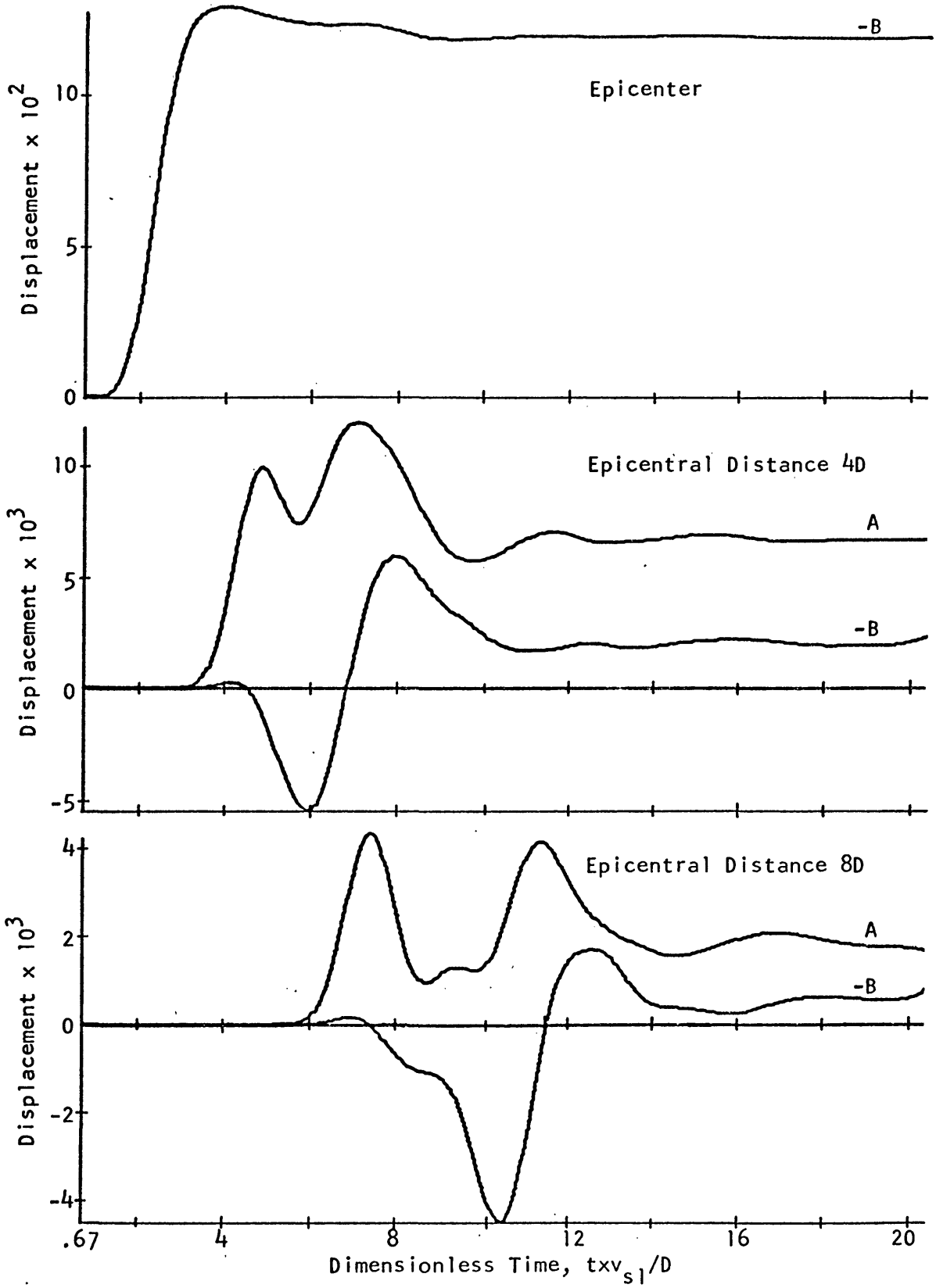

FIGURE 12. Horizontal and Vertical Displacement on the Surface of a Layered Half-Space. A Point Source at Depth D has a Step-like Pulse of Length 3. Layer Thickness 4.375D. Computed with FD2LC. $v_{c1}/v_{c2}=3/4$, $v_{s1}/v_{s2}=5/4$, $v_{s1}/v_{c1}=2/3$, $\rho_1/\rho_2=2/3$.

is quite different for the two cases, Fortran program FD2LC may be considered satisfactory, particularly since it was implemented for model conditions in which $\mu_2 < \mu_1$ and not $\mu_2 \approx \mu_1$.

Three-Layer Models -- Two cases of three-layer models implemented were tested by setting the elastic conditions for layer 1 and 2 equal. The seismograms of the resulting two-layer models were compared with seismograms computed with the proved two-layer program FD2LA.

Case 1: In this case the Lamé constants of the second layer are smaller than those of the first and third layer. Fortran program FD3LBA was designed to treat this case.

Figure 13 shows three seismograms computed with FD3LBA. They are for a model of the earth's crust and upper mantle. A radial space increment of 2 km, a vertical space increment of 1 km, a time increment of 0.075 sec and a source depth of 8 km was chosen. The displacement pulse of the point source is step-like, i.e., the near field-term of the complete pulse with a step-like source potential. The rise time of the step is 6 seconds.

Figure 13 should be compared with Figure 17, which is for the same model conditions but computed with Fortran program FD2LA. The agreement is perfect, except for the very end of the seismograms. This portion, however, is affected by the arrival of the grid-boundary reflection and is not a true

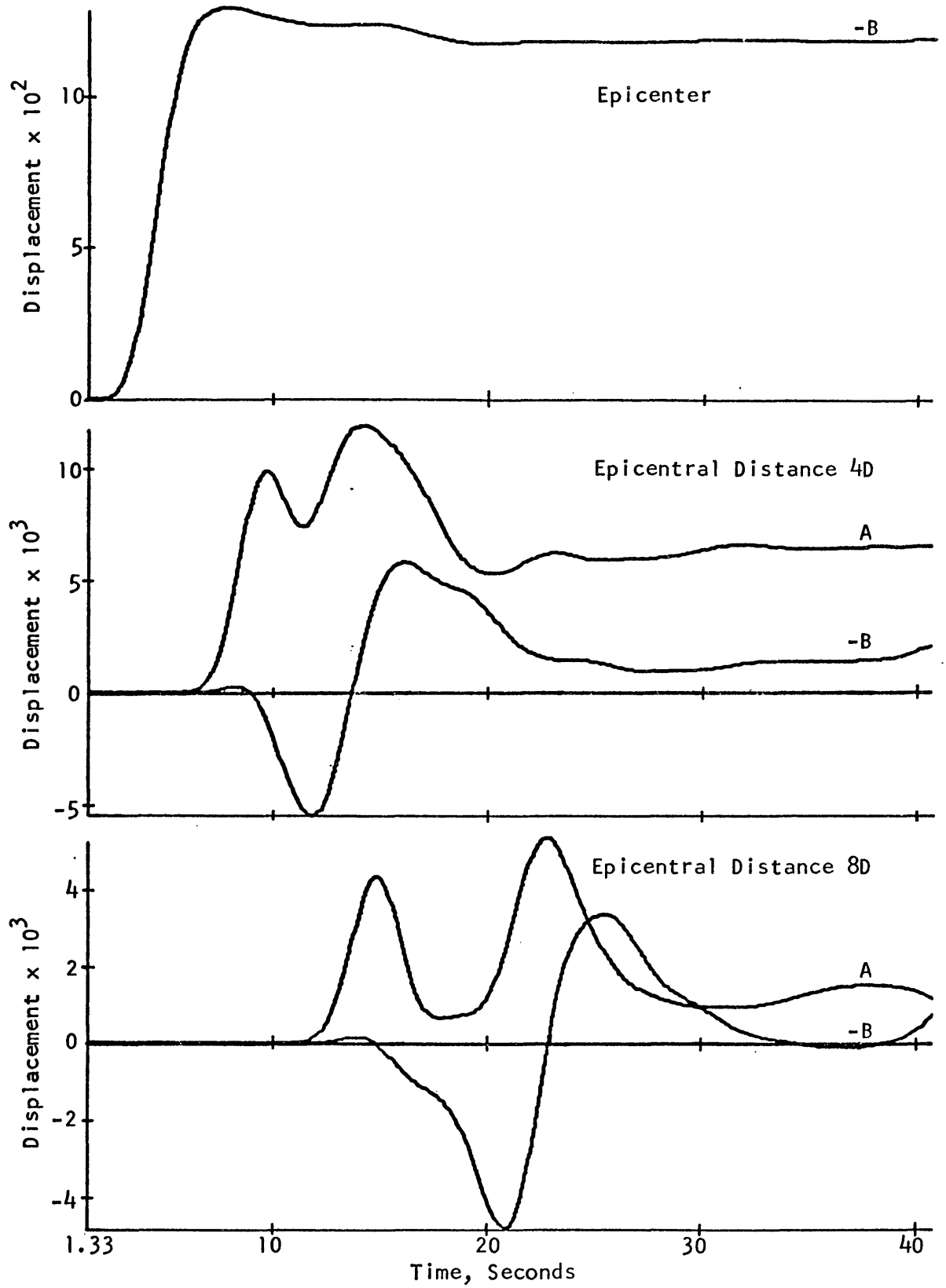

FIGURE 13. Horizontal and Vertical Displacement on the Surface of a Layered Half-Space. A Point Source at D= 8 km has a Step-like Pulse of 6-sec Length. Layer 1: v_{c1}=6km/sec, v_{s1}=4km/sec, ρ_1=3gm/cm^3, 30km; Layer 2: v_{c2}=6km/sec, v_{s2}=4km/sec, ρ_2=3gm/cm^3,5km; Half-Space: v_{c3}=8km/sec, v_{s3}=4.5km/sec, ρ_3=4.5gm/cm^3; FD3LBA. Computed with

representation of seismic events. The number of grid points for the three-layer program is somewhat smaller than that for the two-layer program. The reason for this difference is that the size of the computational portion of the three-layer program is slightly larger than that of the two-layer program. The difference between the two program lengths is the amount by which the displacement arrays of the three-layer programs had to be shortened.

The computational cycle of Fortran program FD3LBA includes the computation of the interface boundary conditions at interface 1 even though the elastic conditions across this interface do not change for the present model conditions. Thus, these boundary conditions were computed correctly, namely, as if no interface boundary existed at this location. FD3LBA may, therefore, be considered correct.

Case 2: For this case the rigidity of the second layer is smaller than that of the first and the third layer. The second model condition is $\rho_1 v_{c1}^2 \leq \rho_2 v_{c2}^2 \leq \rho_3 v_{c3}^2$. Fortran program FD3LCA was implemented for this case.

Figure 14 shows three seismograms computed with FD3LCA. The elastic and model parameters were the same as those used to obtain Figure 13. A comparison with Figure 17 shows that the statements made for Case 1 are true, as well for the present case. Thus, FD3LCA may be considered correct.

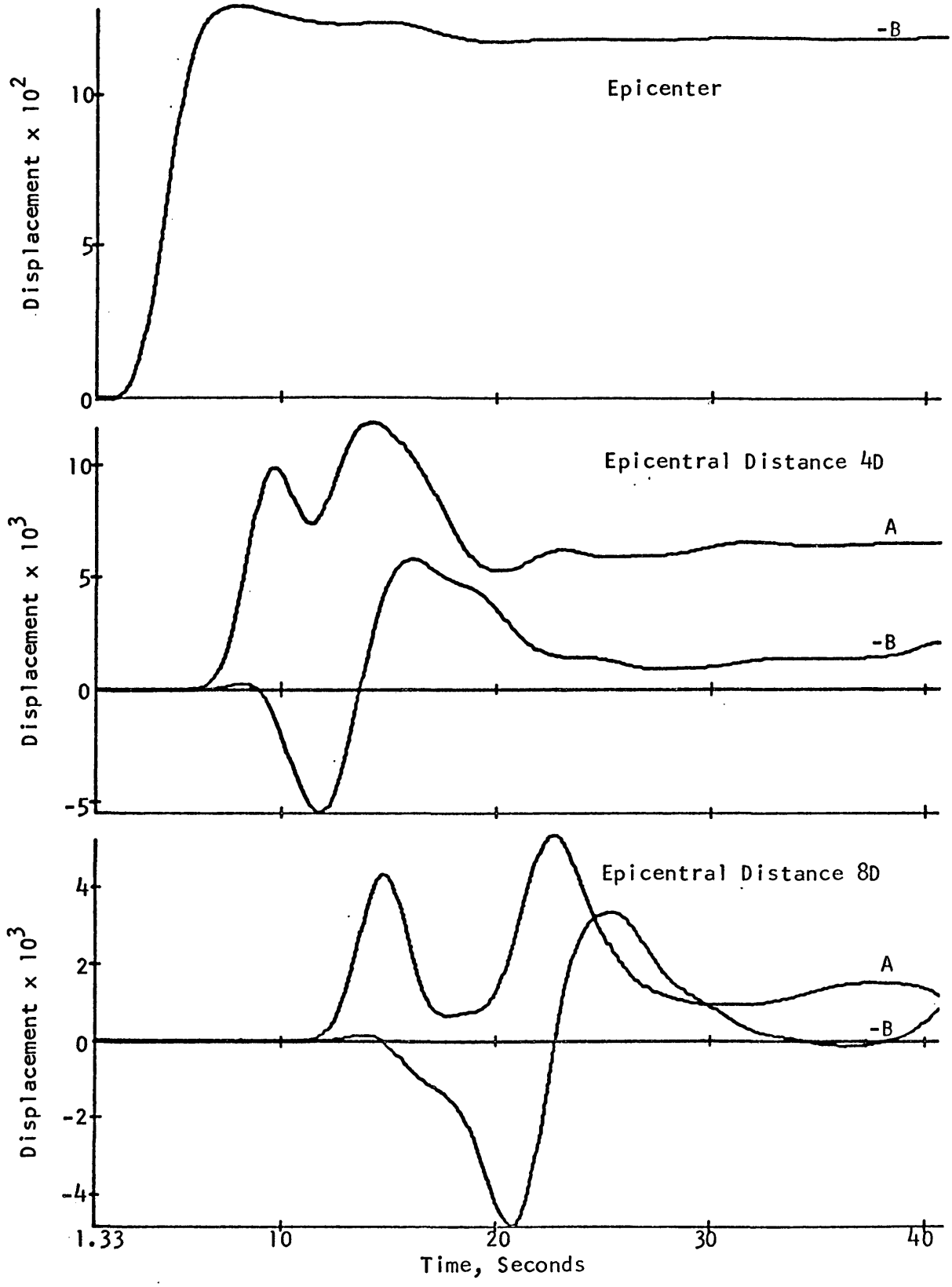

FIGURE 14. Horizontal and Vertical Displacement on the Surface of a Layered Half-Space. A Point Source at D= 8 km has a Step-like Pulse of 6-sec Length. Layer 1: v_{c1}=6km/sec, v_{s1}=4km/sec, ρ_1=3gm/cm^3, 30km; Layer 2: v_{c2}=6km/sec, v_{s2}=4km/sec, ρ_2=3gm/cm^3, 5km; Computed with Half-Space: v_{c3}=8km/sec, v_{s3}=4.5km/sec, ρ_3=4.5gm/cm^3; FD3LCA.

INVESTIGATION OF DISPLACEMENT STEPS

Presented in this chapter is an investigation of the propagation of a step-like displacement pulse in models of the earth's crust and upper mantle. The main interest lies in the effect of a variation of the rigidity in the upper mantle or in the lower crust, on the attenuation with distance from the source of the remnant displacement of the step-like pulse.

The attenuation of the remnant displacement of a step-like displacement pulse was studied on the model of a homogeneous, isotropic half-space, on two-layer and on three-layer models of varying rigidities in the second layer. Throughout this entire investigation, the elastic conditions in the first layer were held constant and equal to those used in the investigation of the half-space model.

To avoid undue complexities in the synthetic seismograms due to strong transient waves, which are of no immediate interest to the present research, the near field term of the complete source pulse (Fig. 2) was chosen for this investigation. The source performs a continuous radial expansion to a maximum amplitude, at which it remains after a rise time of 6 seconds. This comparatively long rise time was necessary to avoid Gibbs oscillations in the synthetic seismograms because of coarse sampling. To obtain a larger spatial coverage in radial direction without affecting too severely the accuracy of the computation of

the boundary conditions across the horizontal boundaries, a radial space increment of 2 km and a vertical space increment of 1 km was chosen. The time increment was made 0.075 seconds. These parameters together with the elastic conditions chosen to simulate the earth's crust and upper mantle, resulted in smooth and stable synthetic seismograms. The minimum source depth was limited to 8 km by the size of the source region. This source depth was used throughout the investigation to obtain a maximum for the ratio of distance of the receivers from the source to source depth.

One-Layer Model -- Figure 15 shows three synthetic seismograms for a homogeneous isotropic half-space with a compressional wave speed of v_c = 6 km/sec and a shear wave speed of v_s = 4 km/sec. The receivers are located on the surface at epicentral distances of 0, 4 and 8 source depths.

The last graph of figure 15, for an epicentral distance of 8 source depths, shows the compressional wave essentially separated from the Rayleigh wave. The theoretical arrival time for the Rayleigh wave of 17.93 seconds checks well with that of the horizontal component in the seismogram. The horizontal component of the remnant displacement of the step arrives in two parts. The part present after the compressional transient is approximately 16 percent of the total amplitude. The remaining 84 percent is added during the Rayleigh-wave transient.

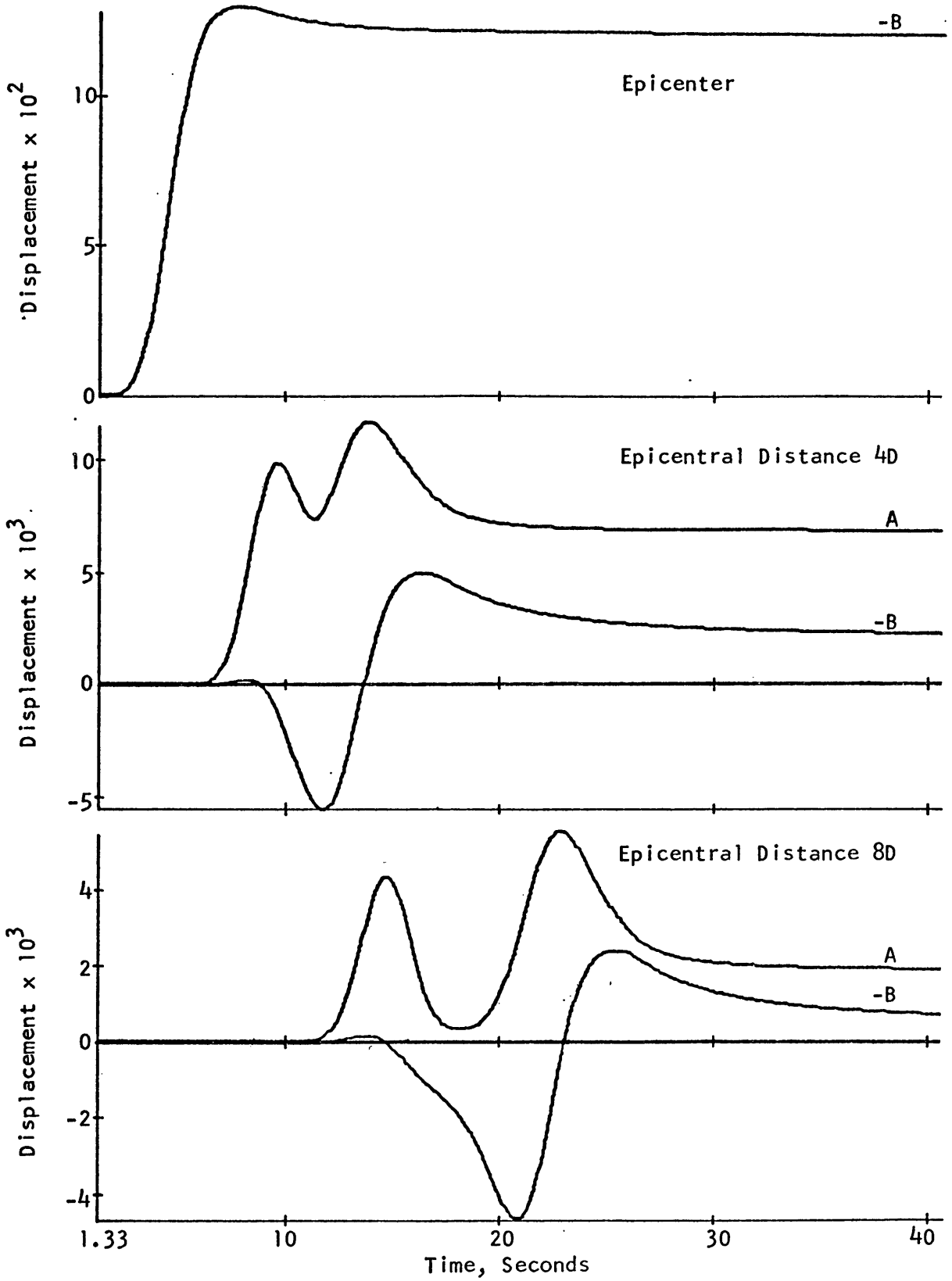

FIGURE 15. Horizontal and Vertical Displacement on the Surface of an Homogeneous Isotropic Half-Space. A Point Source at D= 8 km has a Step-like Pulse of 6-sec Length. v_c=6km/sec, v_s=4km/sec.

The relative compressional wave remnant of the step decreases with the distance from the source. A quantitative relationship for the ratio of compressional wave to Rayleigh wave remnant of the step could not be established for lack of data.

Figure 16 shows plots of the total and horizontal remnant of the displacement step versus distance from the source. The theoretical curves for the static displacement components, determined after L. Cagniard (1962), are also shown in this figure. The discrepancies between the exact-static and the finite-difference solution are apparently primarily caused by the short time to which the computation of the seismograms could be carried in the finite-difference case. The displacements for the finite-difference case are plotted for the time t = 39.5 seconds, at which the radius of the compressional wave front is 237 km. The Rayleigh wave has progressed to a radius of 141 km from the epicenter. It is apparent in Figure 15 that there is still a relaxation of the displacements in progress at the end of the seismograms. This condition is particularly true for the vertical displacement components.

Two-Layer Model -- The two-layer model of the crust and upper mantle was investigated for three different rigidities of the mantle. The crustal elastic parameters are the same for all of the three cases, namely v_{c1} = 6 km/sec, v_{s1} = 4 km/sec,

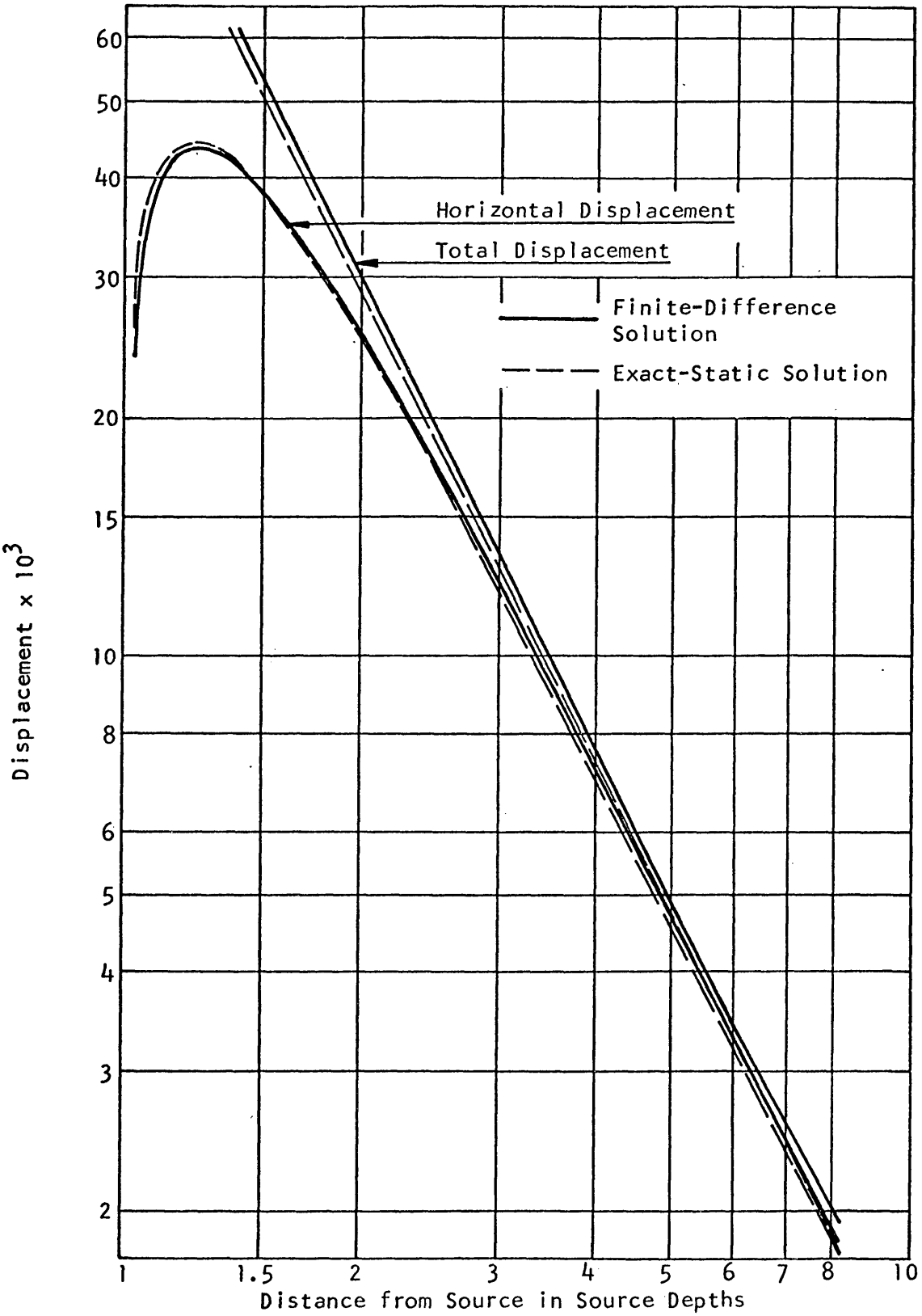

FIGURE 16. Total and Horizontal Remnant Displacement of a Step-like Pulse on the Surface of a Homogeneous Isotropic Half-Space versus Distance from a Point Source.

$\rho_1 = 3$ gm/cm^3. The compressional wave speed $v_{c2} = 8$ km/sec and the density $\rho_2 = 4.5$ gm/cm^3 of the mantle are also the same for all of the investigated cases.

Figure 17 shows three seismograms for points on the surface at epicentral distances of 0, 4, and 8 source depths. The shear wave speed of the mantle is $v_{s2} = 4.5$ km/sec. In the first two graphs, body events and Rayleigh waves are well attenuated; the remnant displacement can be observed excellently in the second half of the synthetic seismograms. This is also true for all seismograms to epicentral distances of 7D. The horizontal traces of the seismograms for epicentral distances of 6 and 7 source depths show essentially constant amplitude from approximately 32 and 34 seconds on, respectively, following the last rise of the long-period Rayleigh wave. This constant displacement is apparently the remnant step displacement, also seen in the last graph of Figure 17. The downward trend at the end is caused by the boundary reflection which arrives at approximately 39 seconds. Figure 22 shows the plot of the horizontal amplitude of the remnant displacement versus the distance from the source on the surface of the layered half space. Figure 23 shows the same relationship for the total remnant displacement. Between the epicenter and an epicentral distance of 6 source depths, the total remnant displacement attenuates with a relationship $R^{-2.1}$ for $v_{s2} = 4.5$ km/sec.

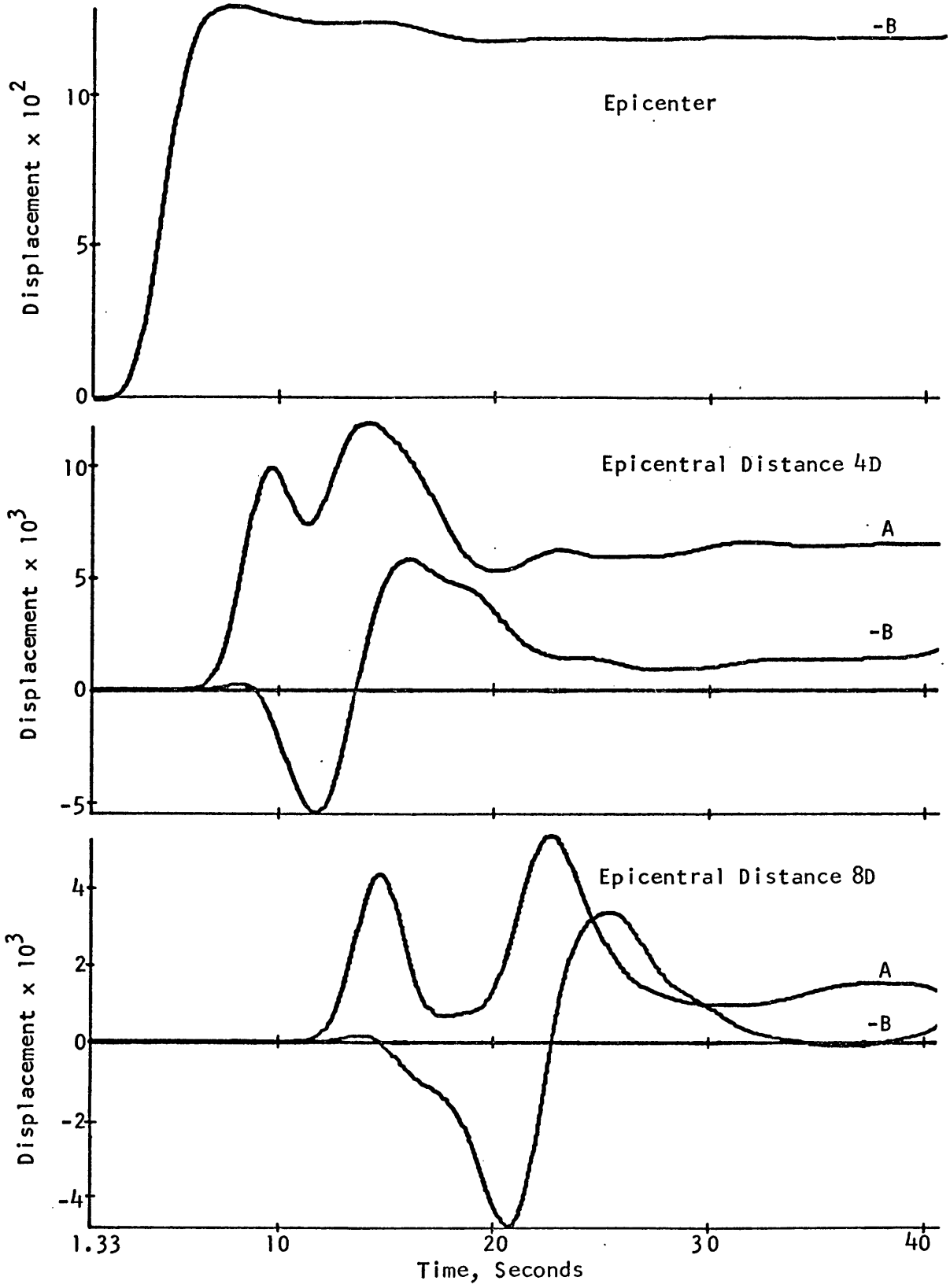

FIGURE 17. Horizontal and Vertical Displacement on the Surface of a Layered Half-Space. A Point Source at D= 8 km has a Step-like Pulse of 6-sec Length. Layer: v_{c1}=6km/sec, v_{s1}=4km/sec, ρ_1=3gm/cm^3, 35km; Half-Space: v_{c2}=8km/sec, v_{s2}=4.5km/sec, ρ_2=4.5gm/cm^3.

From an epicentral distance of 6 source depths on, the slope of the curve decreases to $R^{-2.5}$ between 7 and 8 source depths epicentral distance, indicating stronger attenuation. This effect may be due to the closer proximity of these points to the progressing compressional wave front and the Rayleigh wave train.

As in the case of the half-space, most of the remnant displacement seems to arrive during the passage of the large-amplitude Rayleigh wave. In the last graph of Figure 17, the primary compressional pulse and the Rayleigh wave are well separated. The amplitude between these two phases is higher than in the half-space case. This increase in amplitude -- perhaps caused by the reflected compressional wave, which arrives at $t = 14.8$ seconds -- may also indicate the beginning of the arrival of the step, since the arrival time of the very long-period Rayleigh waves ($T \rightarrow \infty$) is 15.4 sec, well within the primary compressional pulse.

Figure 18 shows three synthetic seismograms for three points on the surface of the layered half-space at the epicenter and for epicentral distances of four and eight source depths. The shear-wave speed of the mantle for this case is $v_{s2} = 3.2$ km/sec. The remnant displacement, well recognized in the second half of the synthetic seismogram, again arrives during the passage of the large-amplitude Rayleigh-wave.

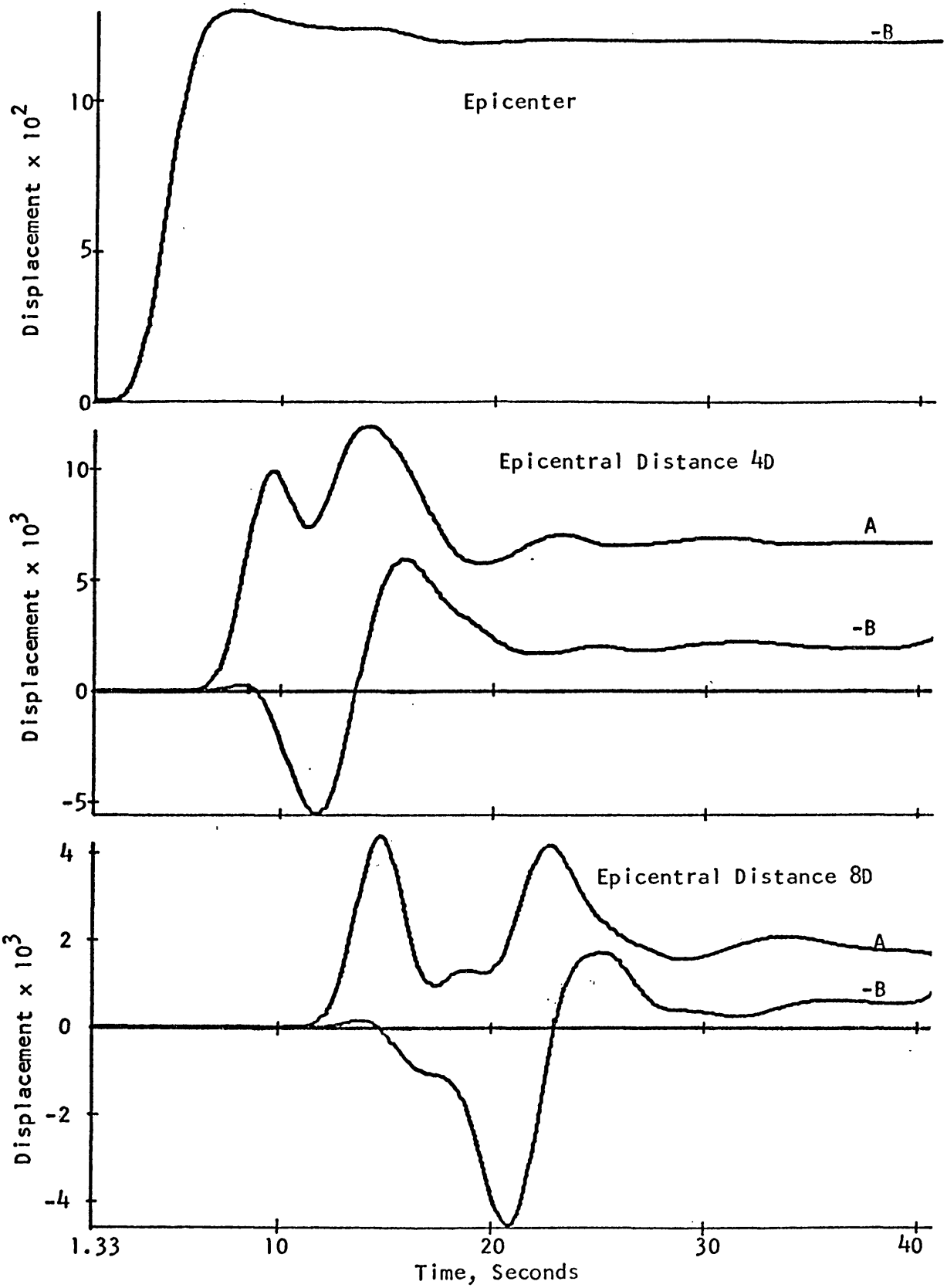

FIGURE 18. Horizontal and Vertical Displacement on the Surface of a Layered Half-Space. A Point Source at D = 8 km has a Step-like Pulse of 6-sec Length. Layer: v_{c1}=6km/sec, v_{s1}=4km/sec, ρ_1=3, 35 km thick; Half-Space: v_{c2}=8km/sec, v_{s2}=3.2km/sec, ρ_2=4.5.

The horizontal and total amplitudes of the remnant displacement are plotted in Figures 22 and 23, respectively, for v_{s2} = 3.2 km/sec. A definite change of the amplitude-to-distance relationships from the previous case can be observed, from an epicentral distance of two source depths on. For the total displacement, this relationship is $R^{-2.0}$ from epicentral distances of 1 to 5 source depths. It changes to $R^{-1.7}$ from epicentral distances of 7 to 8 source depths. This change in amplitude-to-distance relationship from the previous case is apparently caused by the lower shear-wave speed in the second layer in the present case. For the present case the ratio of rigidities is μ_2/μ_1 = 0.96 as compared with μ_2/μ_1 = 1.898 for the previous case.

Figures 19, 20, and 21 show a complete suite of synthetic seismogram for points on the surface at epicentral distances from 0 to 8 source depths in increments of one source depth. The shear-wave speed of the mantle for this case is v_{s2} = 1.5 km/sec. A considerable change in wave forms of the Rayleigh-wave train occurs in this case, as compared with the two previous cases. The Rayleigh wave appears to describe a more nearly resonant phenomenon, from an epicentral distance of three source depths upward. The second trough deepens and a following peak developes; these excursions occur about a distinctly higher remnant displacement level. This effect can be well traced throughout the seismograms for epicentral distances from 3 to 8 source depths.

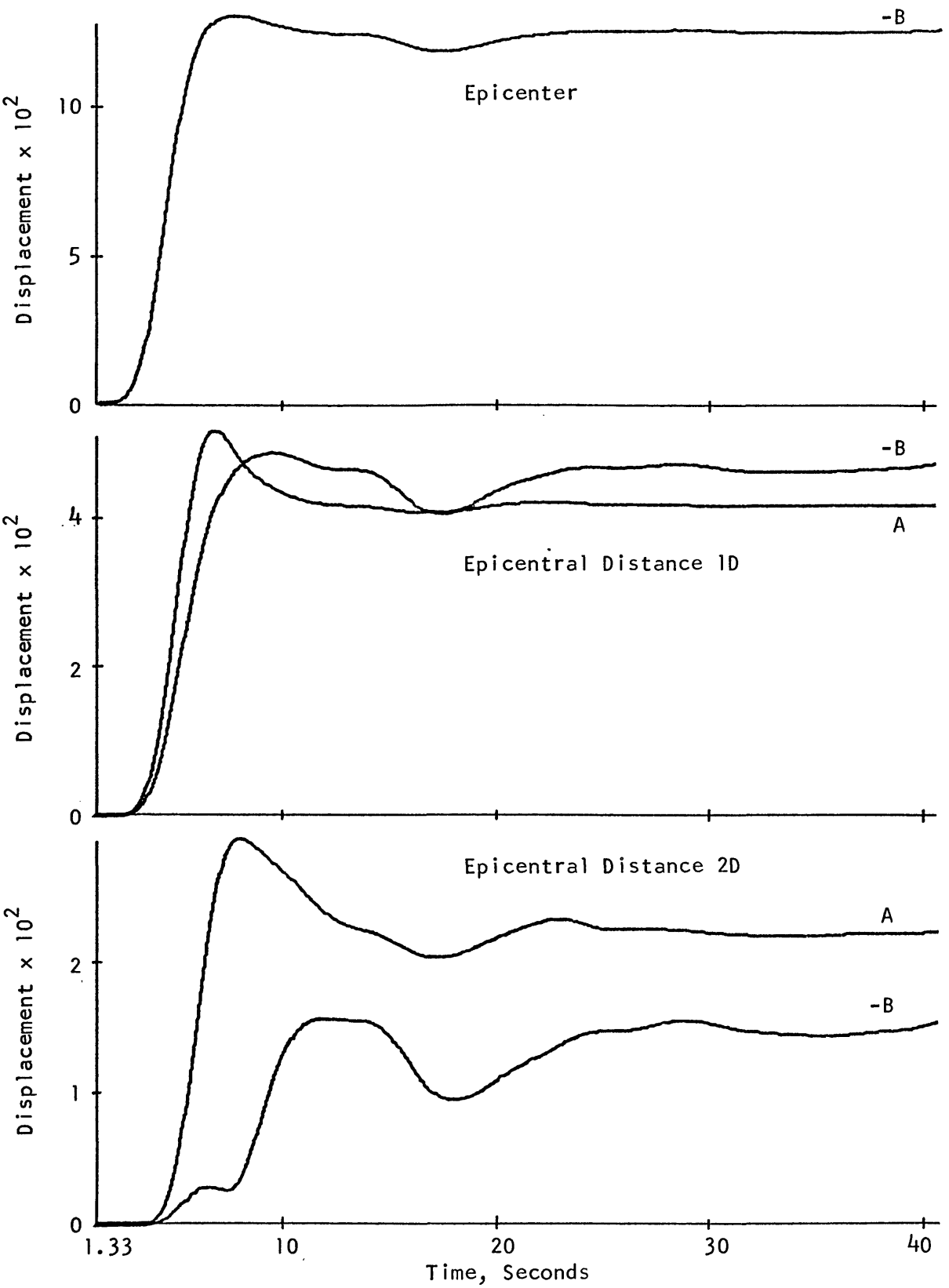

FIGURE 19. Horizontal and Vertical Displacement on the Surface of a Layered Half-Space. A Point Source at D = 8 km has a Step-like Pulse of 6-sec Length. Layer: v_{c1}=6km/sec, v_{s1}=4km/sec, ρ_1=3gm/cm^3, 35km; Half-Space: v_{c2}=8km/sec, v_{s2}=1.5km/sec, ρ_2=4.5 gm/cm^3.

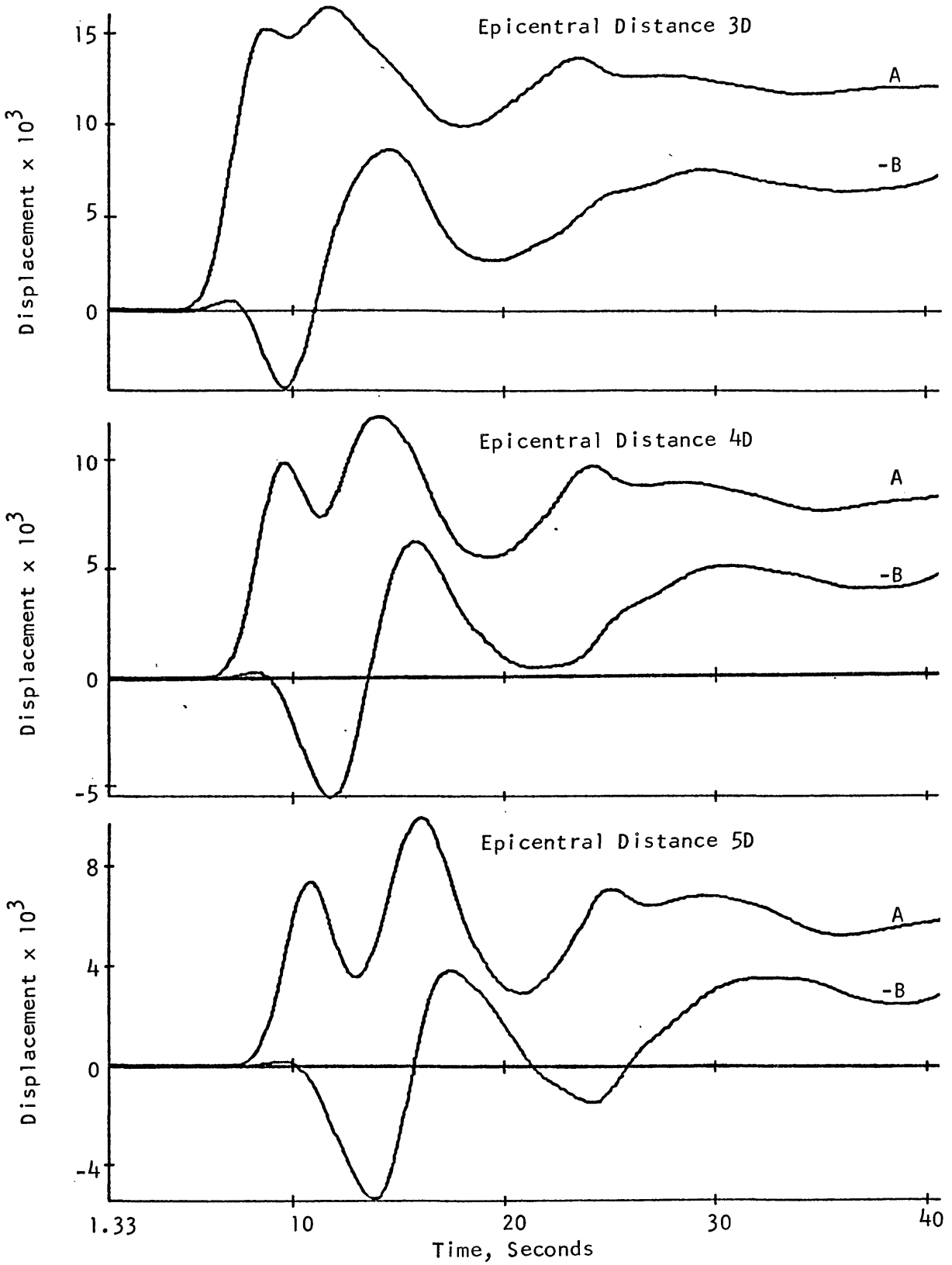

FIGURE 20. Horizontal anf Vertical Displacement on the Surface of a Layered Half-Space. A Point Source at D = 8 km has a Step-like Pulse of 6-sec Length. Layer: v_{c1}=6km/sec, v_{s1}=4km/sec, ρ_1=3gm/cm^3, 35km; Half-Space: v_{c2}=8km/sec, v_{s2}=1.5km/sec, ρ_2=4.5gm/cm^3.

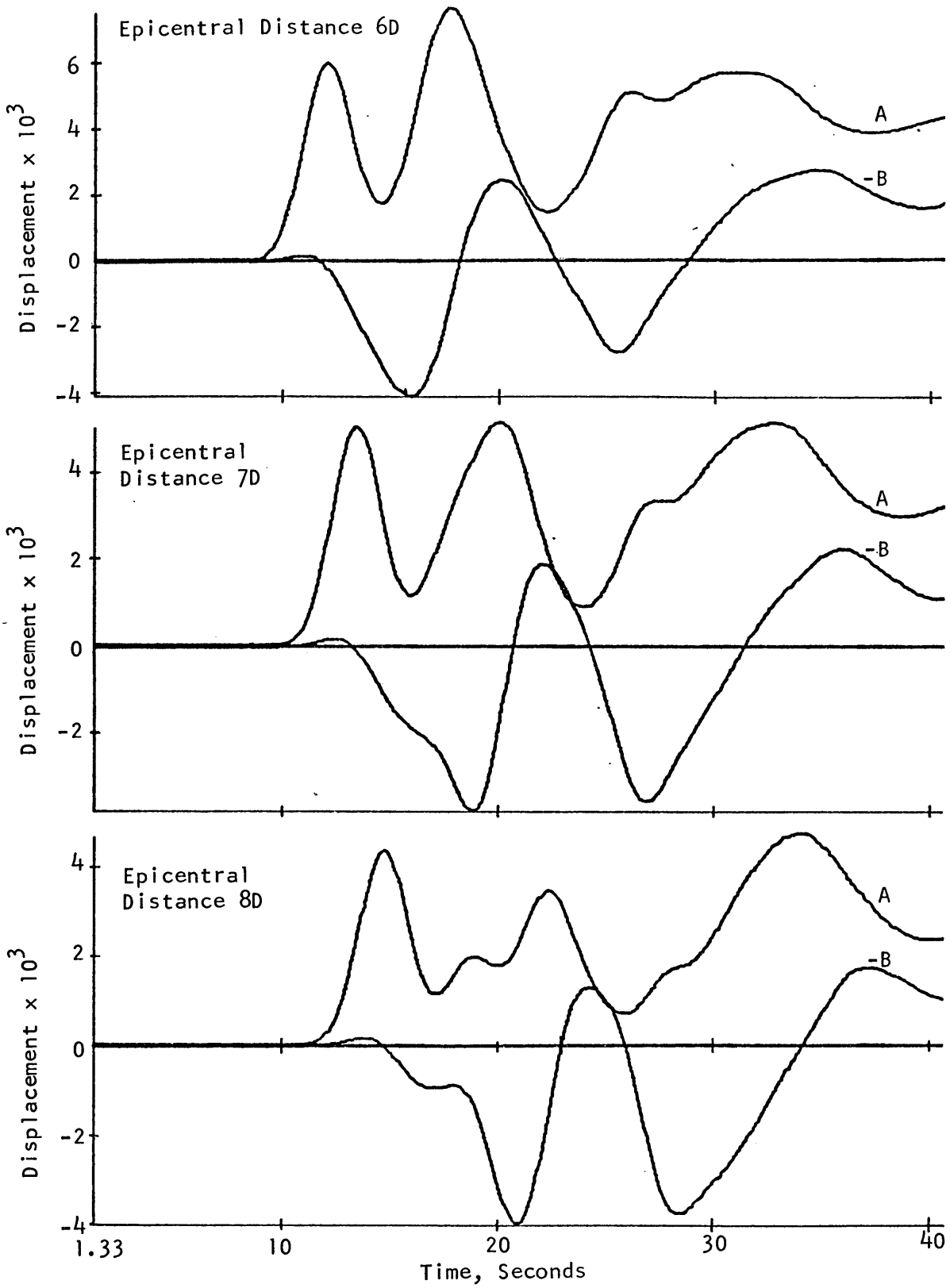

FIGURE 21. Horizontal and Vertical Displacement on the Surface of a Layered Half-Space. A Point Source at D = 8 km has a Step-like Pulse of 6-sec Length. Layer: v_{c1}=6km/sec, v_{s1}=4km/sec, ρ_1=3gm/cm^3, 35km; Half-Space: v_{c2}=8km/sec, v_{s2}=1.5km/sec, ρ_2=4.5gm/cm^3.

The horizontal and total amplitudes of the remnant displacement are also plotted in Figures 22 and 23, for v_{s2} = 1.5 km/sec. The remnant displacements were calculated as the average between peak and trough of the final Rayleigh-wave oscillations. A very pronounced change of the amplitude-to-distance relationship can be observed from the two previous cases. For the total displacement, this relationship is $R^{-1.8}$ between epicentral distances of 1 and 3 source depths, which changes to $R^{-1.1}$ between epicentral distances of 7 and 8 source depths. The amplitude-to-distance relationship for the horizontal remnant displacement changes from $R^{-1.7}$ between epicentral distances of 2 and 3 source depths to $R^{-1.0}$ between epicentral distances of 7 and 8 source depths.

Three-Layer Models -- Figures 22 and 23 demonstrate that the geometric attenuation of the remnant displacement of a displacement step on the surface of a layered half-space decreases with decreasing rigidity in the second layer. From empirically established Rayleigh-wave despersion curves (Gutenberg [1932], and others), we know, however, that the shear-wave speed in the upper mantle is of the order of 4.5 km/sec, for periods from 7 to 70 seconds. For this shear-wave speed in the second layer, the two-layer model behaves essentially like a homogeneous isotropic half-space, with regard to the geometric attenuation of the remnant displacement.

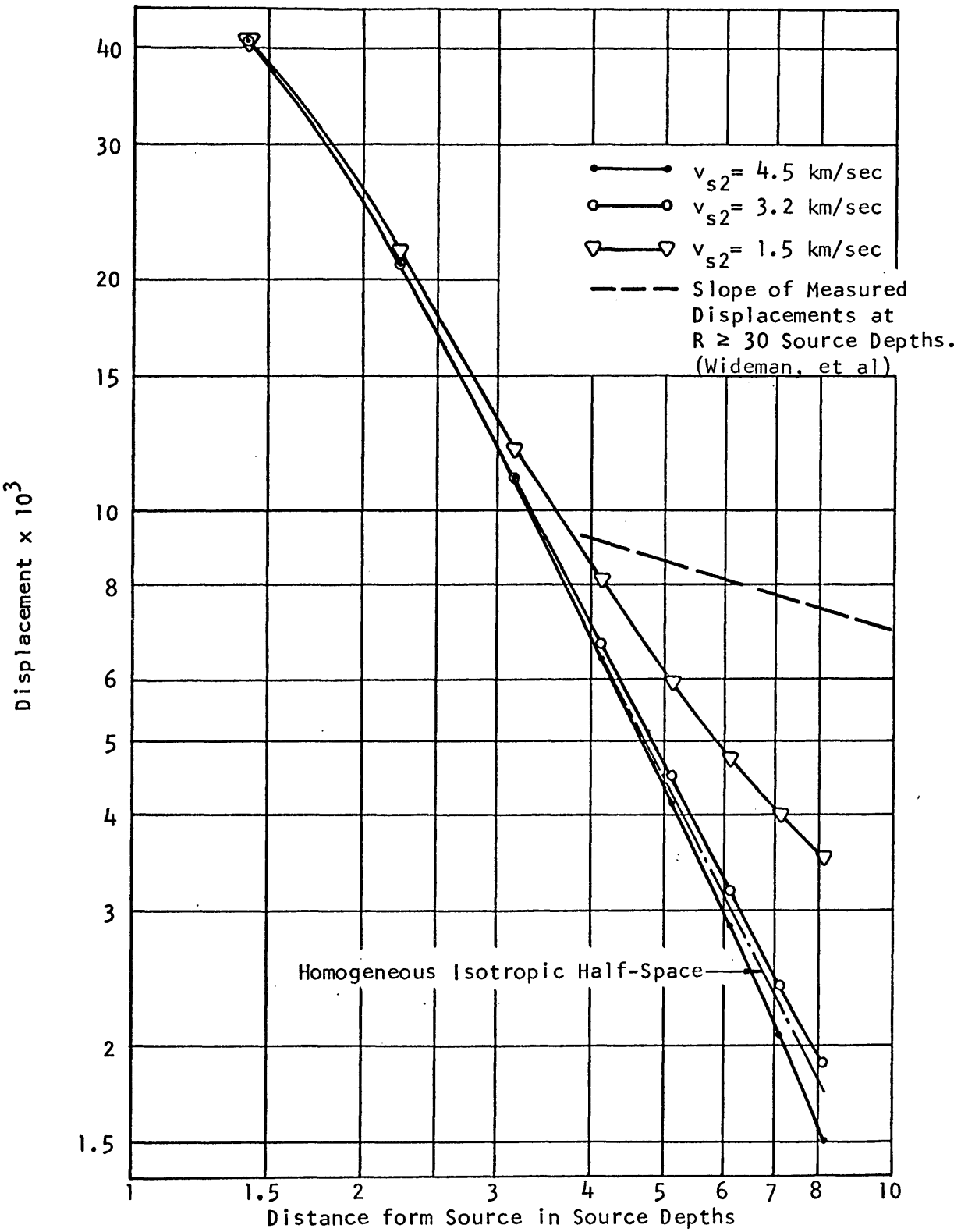

FIGURE 22. Horizontal Remnant Displacement of a Step-like Pulse on the Surface of three Layered Half-Spaces. Layer: v_{c1}= 6 km/sec, v_{s1}= 4 km/sec, ρ_1= 3 gm/cm^3, 35 km; v_{c2}= 8 km/sec, ρ_2= 4.5 gm/cm^3.

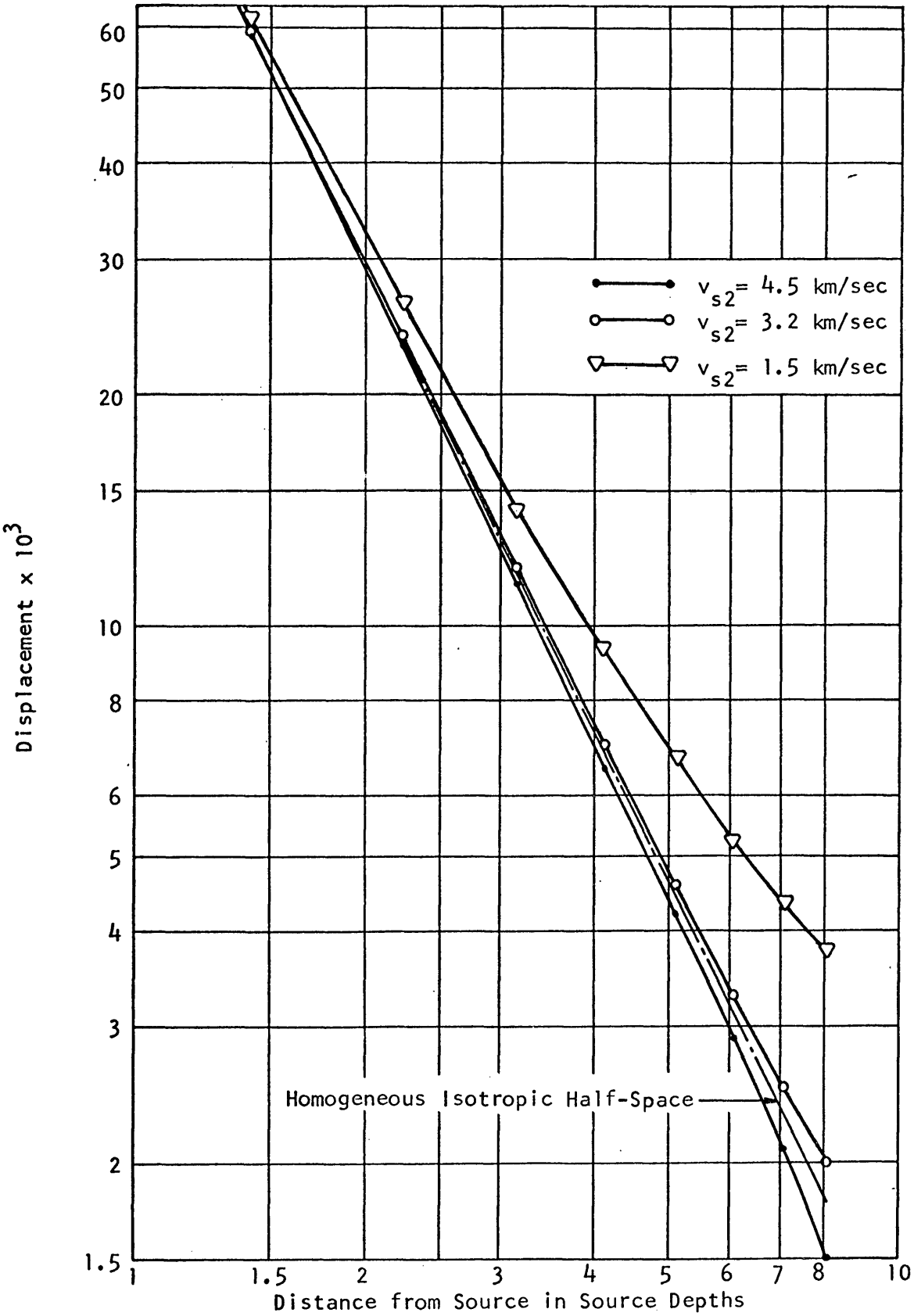

FIGURE 23. Total Remnant Displacement of a Step-like Pulse on the Surface of three Layered Half-Spaces. Layer: v_{c1}= 6 km/sec, v_{s1}= 4 km/sec, ρ_1= 3 gm/cm^3, 35 km; v_{c2}= 8 km/sec, ρ_2= 4.5 gm/cm^3.

Haskell (1953) has calculated Rayleigh-wave dispersion curves for various models of the crust and upper mantle. The following table gives the elastic and geometric parameters of a two-layer and a three-layer model for which Haskell showed that the Rayleigh-wave dispersion curves are almost identical.

	P-wave speed km/sec	S-wave speed km/sec	Density gr/cm^3	Thickness km
Two-layer Model:				
Layer 1	6.14	3.39	2.7	28.38
Half-Space	8.26	4.65	3.0	Infinite
Three-layer Model:				
Layer 1	6.14	3.39	2.7	13.6
Layer 2	5.5	3.18	2.7	11.85
Half-Space	8.26	4.65	3.0	Infinite

Both of these models fit the observed Rayleigh-wave dispersion equally well. This fit indicates that the elastic conditions of the second layer of the three-layer model has little effect on the dispersion curve, as long as the first and the third layer have the same elastic conditions as the two-layer model.

The above conclusions suggested the investigation of three-layer models with a low rigidity in the second layer. The two types of three-layer models investigated correspond to Cases 1 and 2 of page 4.

Case 1: For this case the Lamé constants of the second layer are lower than those of the first and the third layer.

Figure 24 shows three synthetic seismograms for receiver locations on the surface at epicentral distances of 0, 4 and 8 source depths. The elastic and geometric parameters of the model are as follows:

Layer 1: $v_{c1} = 6$ km/sec

$v_{s1} = 4$ km/sec

$\rho_1 = 3$ gm/cm^3

Thickness = 30 km

Layer 2: $v_{c2} = 5.5$ km/sec

$v_{s2} = 3.0$ km/sec

$\rho_2 = 3$ gm/cm^3

Thickness = 5 km

Half-Space: $v_{c3} = 8$ km/sec

$v_{s3} = 4.5$ km/sec

$\rho_3 = 4.5$ gm/cm^3

The last graph of Figure 24 suggests the presence of a long-period Rayleigh wave (approximately 20-sec period) after the passage of the large-amplitude Rayleigh wave. Similar indications were found in the seismograms for epicentral distances from 5 source depths upward not shown in Figure 24. These long-period waves

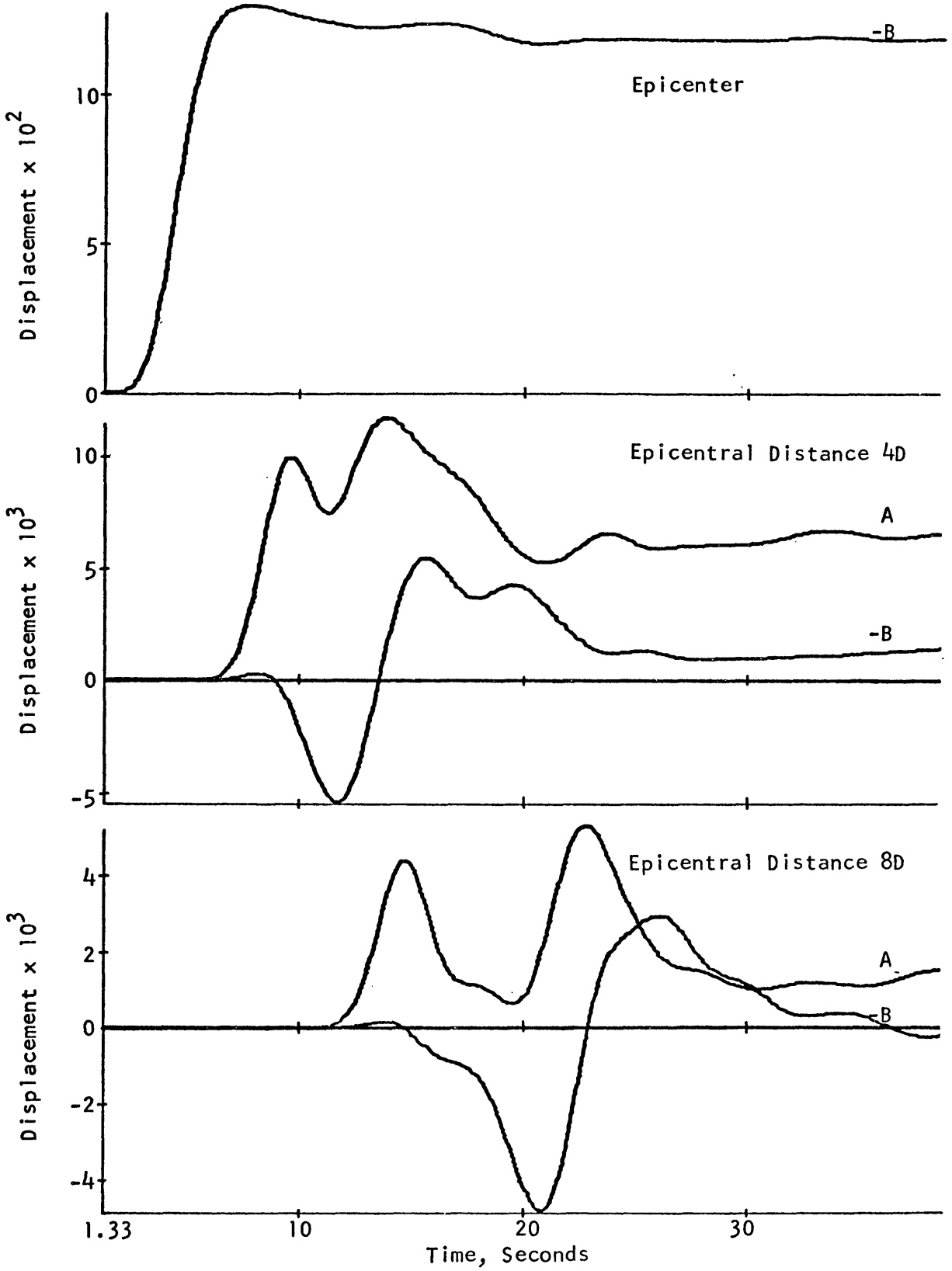

FIGURE 24. Horizontal and Vertical Displacement on the Surface of a Layered Half-Space. A Point Source at D=8km has a Step-like Pulse of 6-sec Length. Layer 1: v_{c1}=6km/sec, v_{s1}=4km/sec, ρ_1=3gm/cm^3, 30km; Layer 2: v_{c2}=5.5km/sec, v_{s2}=3km/sec, ρ_2=3gm/cm^3, 5 km; Half-Space: v_{c3}=8km/sec, v_{s3}=4.5km/sec, ρ_3=4.5gm/cm^3.

made the determination of the remnant displacement of the displacement step impossible. The seismograms are too short to be conclusive.

Figure 25 shows three synthetic seismograms for receivers located on the surface at epicentral distances of 0, 4, and 8 source depths. The elastic and geometric parameters are the same as those for Figure 24, except the shear-wave speed in the second layer, which is v_{s2} = 2 km/sec. The last graph of the figure shows a strong 6.5-sec-period Rayleigh wave after the passage of the large-amplitude Rayleigh wave. This 6.5-sec wave is apparently superimposed on a long-period Rayleigh wave of approximately 20-sec period. This long-period Rayleigh wave again becomes apparent at epicentral distances beyond 5 source depths and masks the remnant displacement of the step. A general increase of the remnant displacement level, over that of the model of Figure 24, seems to be indicated for epicentral distances greater than 5 source depths; however, as before, this level is difficult to define, because of the oscillations. For brevity, intermediate seismograms, computed at increments in epicentral distance of one source depths, are not shown. A quantitative determination of the remnant displacement of the displacement step did not seem to be justified with the present length of the seismograms for epicentral distances larger than four source depths. For epicentral distances smaller than four

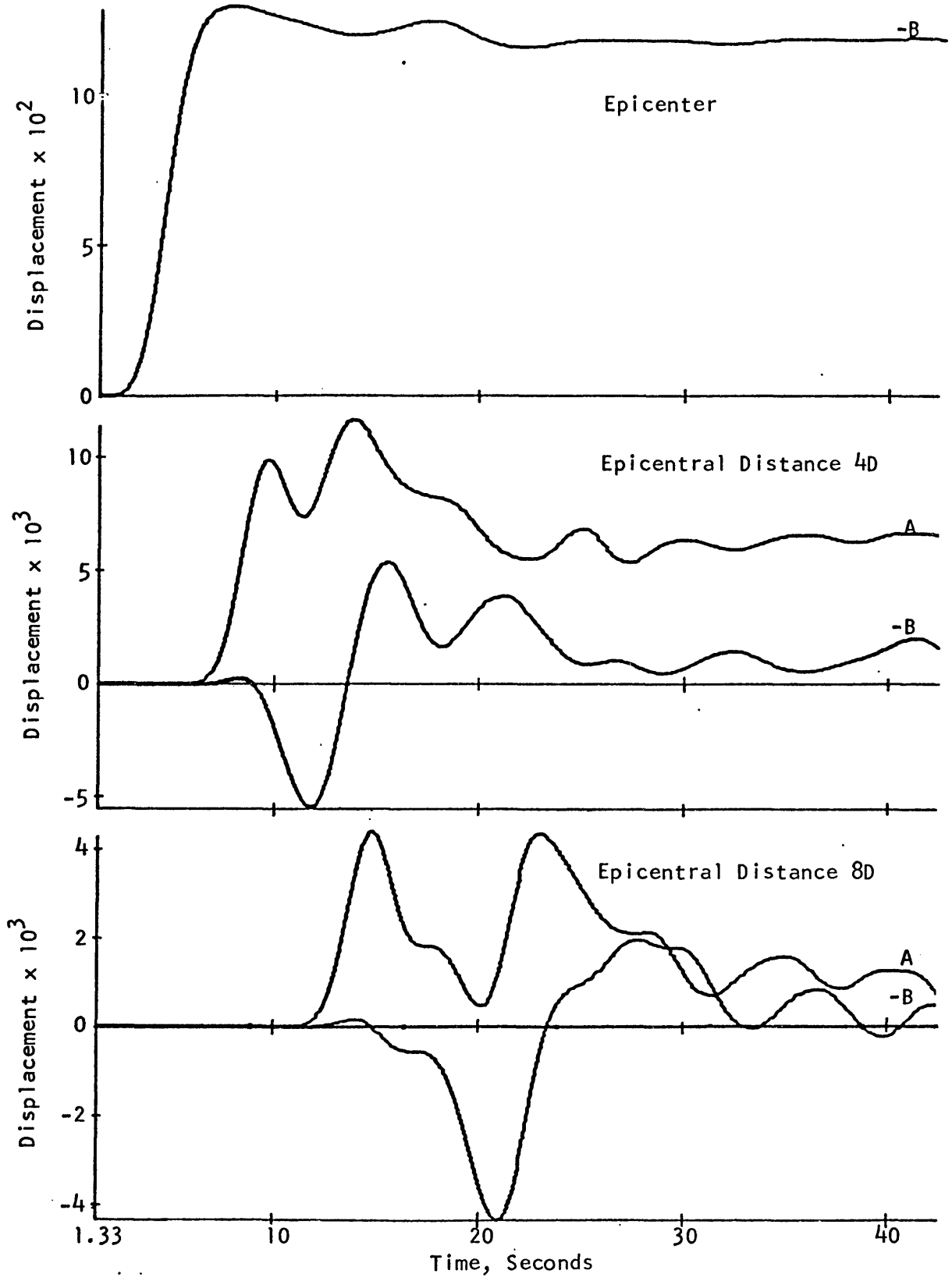

FIGURE 25. Horizontal and Vertical Displacement on the Surface of a Layered Half-Space. A Point Source at D=8km has a Step-like Pulse of 6-sec Length. Layer 1: v_{c1}=6km/sec, v_{s1}=4km/sec, ρ_1=3gm/cm^3, 30 km; Layer 2: v_{c2}=5.5km/sec, v_{s2}=2km/sec, ρ_2=3gm/cm^3, 5 km; Half-Space: v_{c3}=8km/sec, v_{s3}=4.5km/sec, ρ_3=4.5gm/cm^3.

source depths the behavior is close to that of a homogeneous isotropic half-space.

Figure 26 shows three synthetic seismograms for receivers located on the surface at epicentral distances of 0, 4, and 8 source depths. The elastic and geometric parameters are the same as those for Figure 24, except for the shear-wave speed in the second layer, which is v_{s2} = 1 km/sec. The Rayleigh-wave train is more oscillatory in this model than in the two previous cases. A long-period oscillation of 30- to 40-sec period is suggested in the last graph of Figure 26. The interference pattern at approximately 35 sec in the same graph seems to be caused by the constructive interference of several body events.

The events beyond 40 sec should be ignored because of the arrival of the outer-boundary reflections. A quantitative evaluation of the remnant displacement of the displacement step for epicentral distances from 5 source depths up cannot be made because of the presence of the long-period Rayleigh waves. An increase of the remnant displacement level seems to be indicated, however, when Figures 25 and 26 are compared.

Case 2: For this case the elastic conditions are as follows: $\mu_1 > \mu_2 < \mu_3$ and $\rho_1 v_{c1}^2 < \rho_2 v_{c2}^2 \leq \rho_3 v_{c3}^2$.

Figure 27 shows three synthetic seismograms for receiver locations on the surface at epicentral distances of

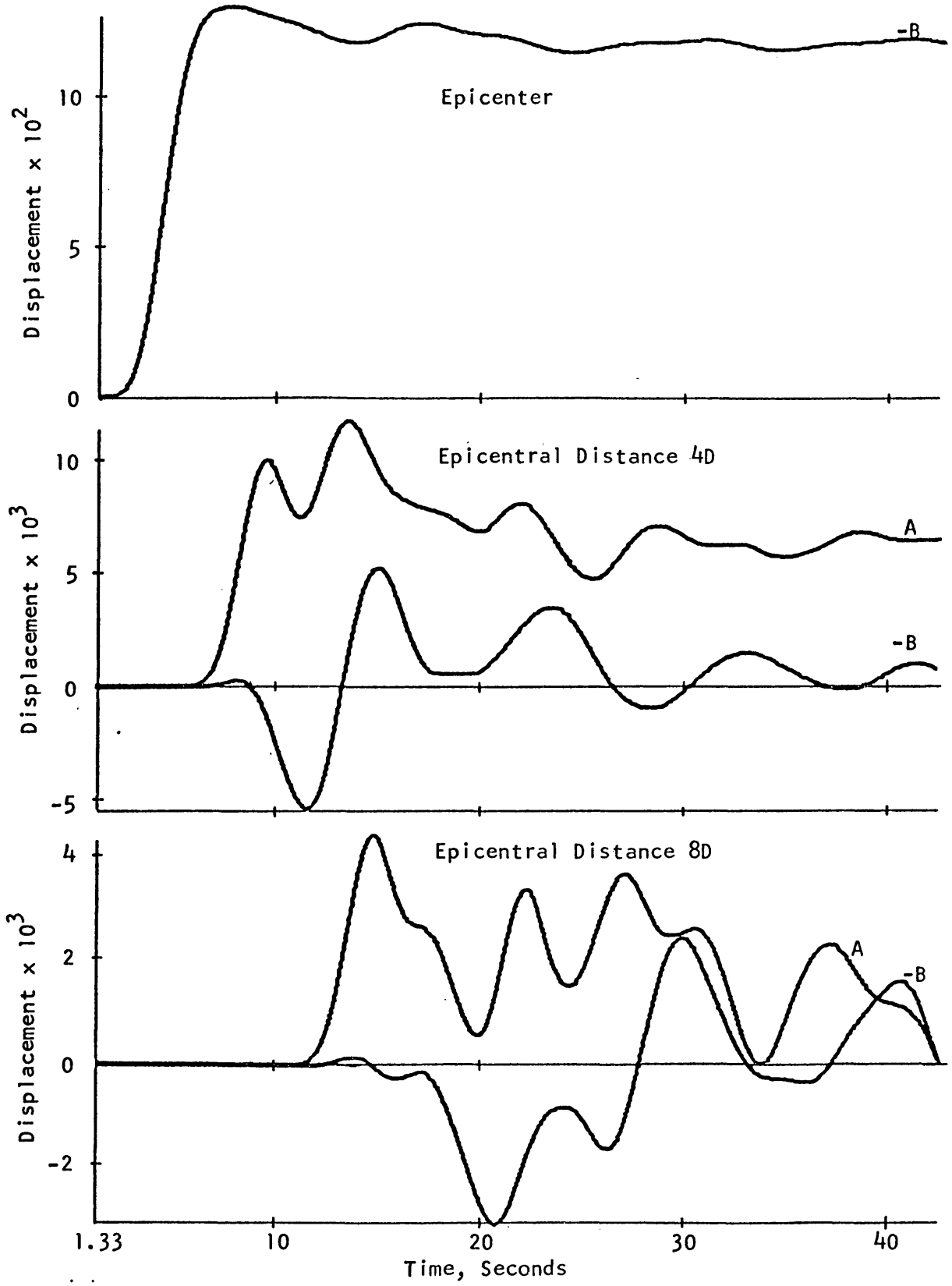

FIGURE 26. Horizontal and Vertical Displacement on the Surface of a Layered Half-Space. A Point Source at D=8km has a Step-like Pulse of 6-sec Length. Layer 1: v_{c1}=6km/sec, v_{s1}=4km/sec, ρ_1=3 gm/cm^3, 30km; Layer 2: v_{c2}=5.5km/sec, v_{s2}= 1km/sec, ρ_2=3 gm/cm^3, 5 km; Half-Space: v_{c3}=8km/sec, v_{s3}=4.5km/sec, ρ_3=4.5 gm/cm^3.

o, 4, and 8 source depths. The elastic and geometric parameters of the model are as follows:

Layer 1: v_{c1} = 6 km/sec
v_{s1} = 4 km/sec
ρ_1 = 3 gm/cm^3
Thickness = 30 km

Layer 2: v_{c2} = 8 km/sec
v_{s2} = 3 km/sec
ρ_2 = 4.5 gm/cm^3
Thickness = 5 km

Half-Space: v_{c3} = 8 km/sec
v_{s3} = 4.5 km/sec
ρ_3 = 4.5 gm/cm^3

The second graph of Figure 27 shows a gradual increase of the displacement to a plateau after the passage of the large-amplitude Rayleigh wave. The same gradual increase to a plateau can also be observed in the last graph and in the seismograms for all points between 4 and 8 source depths epicentral distance not shown here. Assuming that these plateaus comprise the amplitudes of the remnant displacement of the displacement step, its total displacement is related to the distance from the source as $R^{-2.0}$ between 0 and 3 source depths epicentral distance. This relationship changes gradually to $R^{-2.7}$ between epicentral distances of 7 and 8 source depths.

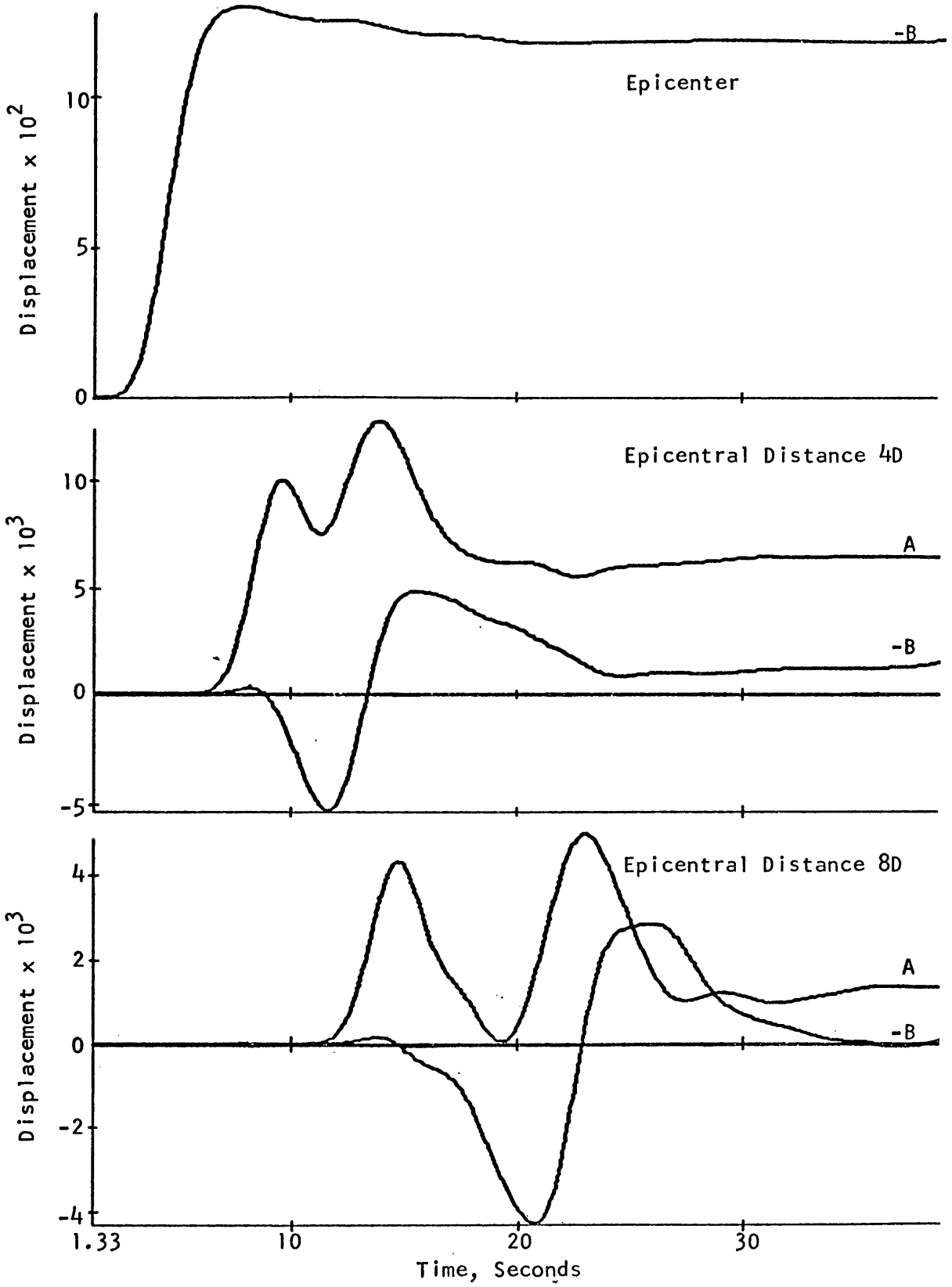

FIGURE 27. Horizontal and Vertical Displacement on the Surface of a Layered Half-Space. A Point Source at D=8km has a Step-like Pulse of 6-sec Length. Layer 1: v_{c1}=6km/sec, v_{s1}=4km/sec, ρ_1=3gm/cm^3, 30km; Layer 2: v_{c2}=8km/sec, v_{s2}=3km/sec, ρ_2=4.5gm/cm^3, 5km; Half-Space: v_{c3}=8km/sec, v_{s3}=4.5km/sec, ρ_3=4.5gm/cm^3.

Figure 28 shows three synthetic seismograms for receiver locations on the surface at epicentral distances of 0, 4, and 8 source depths. The elastic and geometric parameters are the same as for Figure 27, except for the shear-wave speed in layer 2, which is v_{s2} = 2 km/sec. A more oscillatory band of Rayleigh waves is induced here, than in the previous case. As in Case 1, Rayleigh waves of approximately 20-sec period seem to emerge at epicentral distances beyond four source depths, which mask the remnant displacement of the displacement step. A quantitative interpretation of the remnant displacement is, therefore, not possible.

Figure 29 shows three synthetic seismograms for receiver locations on the surface at epicentral distances of 0, 4, and 8 source depths. The elastic and geometric parameters are the same as for Figure 27, except for the shear-wave speed in layer 2, which is v_{s2} = 1 km/sec. In the last graph of the figure, a Rayleigh wave of approximately 16-sec period can be detected upon which are superimposed the very large-amplitude 6- to 11-sec waves. Similar conditions prevail in the seismograms from four source depths epicentral distance upward, which are not shown in Figure 29. A quantitative interpretation of the amplitude of the remnant displacement is, therefore, not possible.

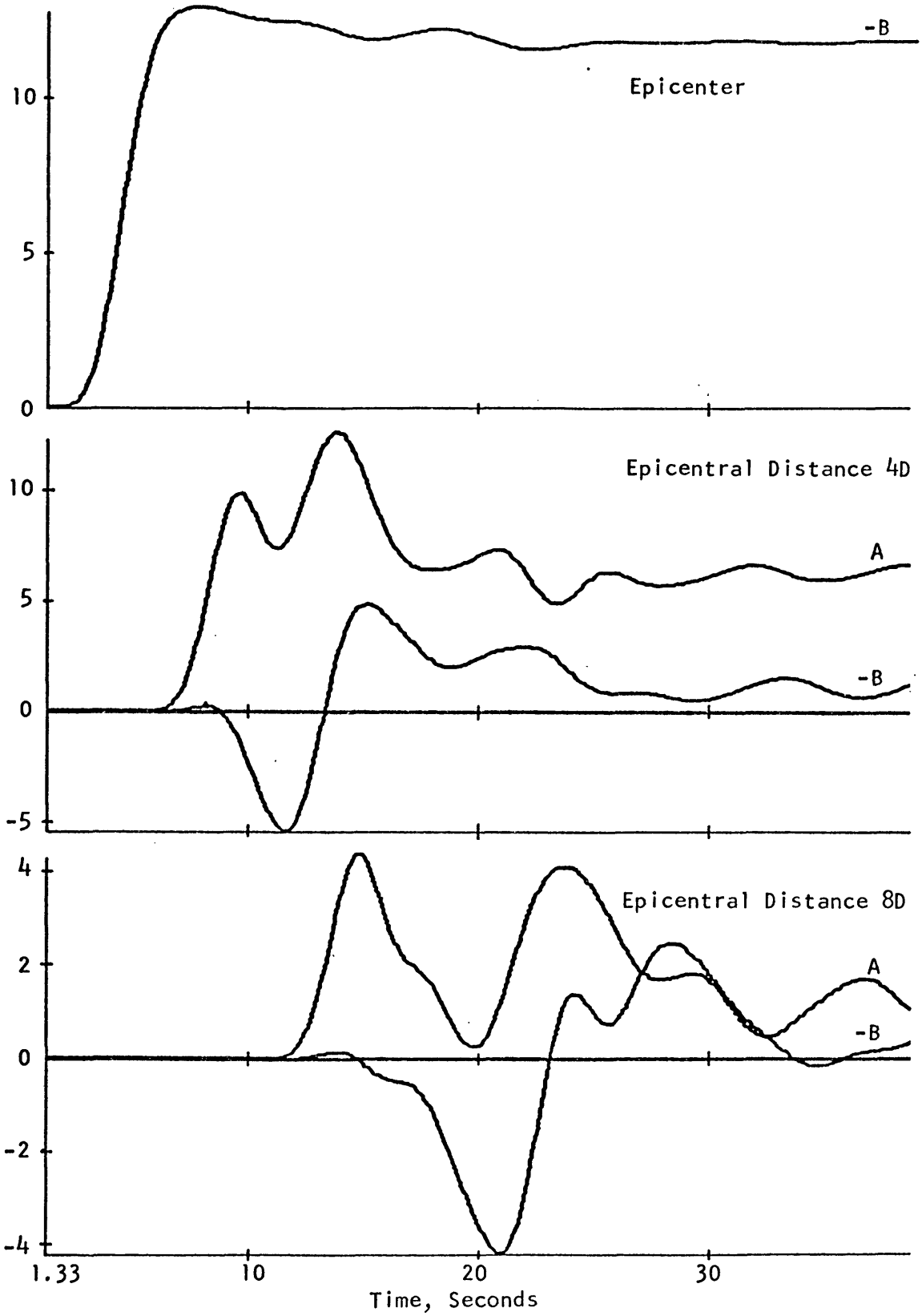

FIGURE 28. Horizontal and Vertical Displacement on the Surface of a Layered Half-Space. A Point Source at D=8km has a Step-like Pulse of 6-sec Length. Layer 1: v_{c1}=6km/sec, v_{s1}=4km/sec, ρ_1=3gm/cm^3, 30km; Layer 2: v_{c2}=8km/sec, v_{s2}=2km/sec, ρ_2=4.5gm/cm^3, 5 km; Half-Space: v_{c3}=8km/sec, v_{s3}=4.5km/sec, ρ_3=4.5gm/cm^3.

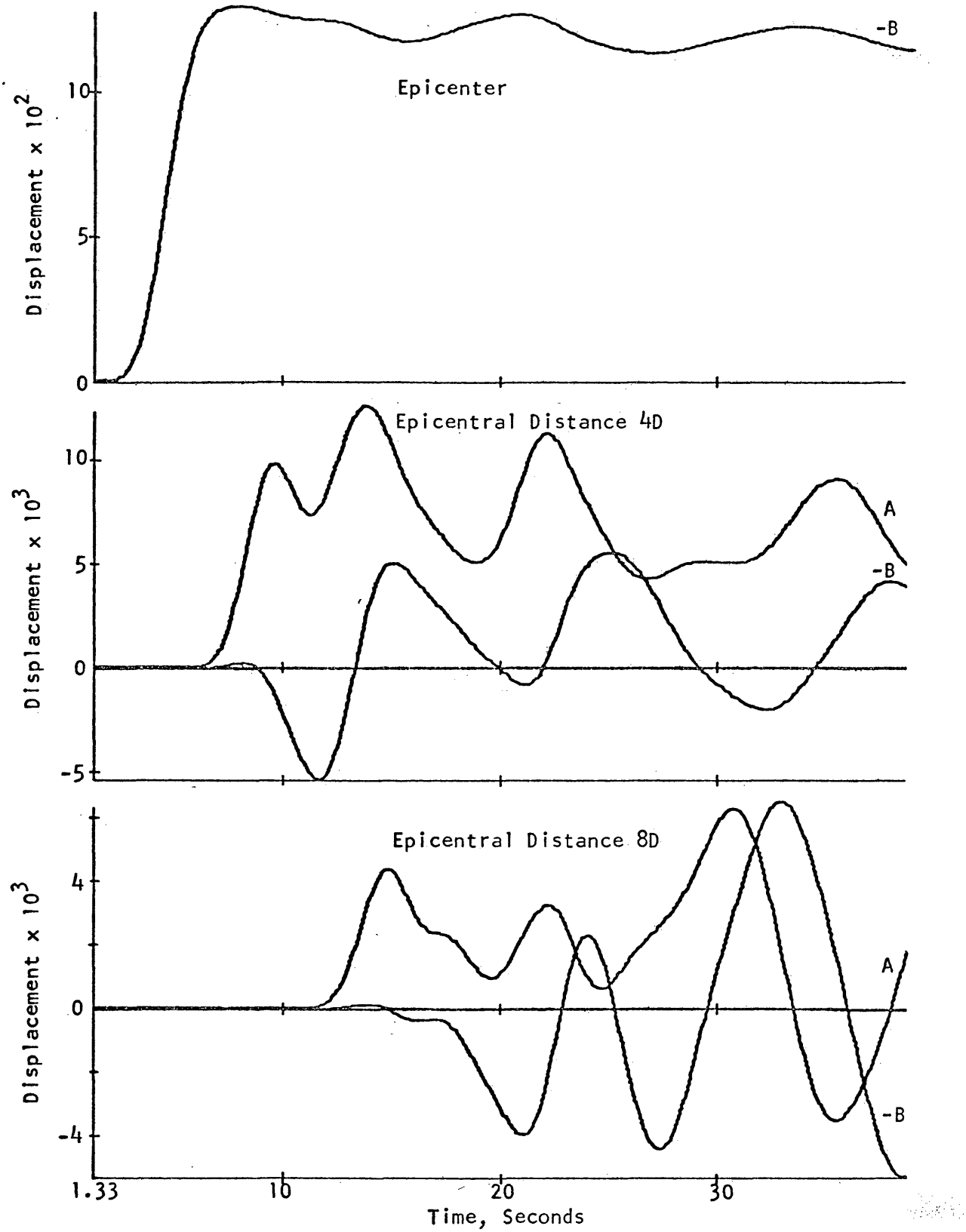

FIGURE 29. Horizontal and Vertical Displacement on the Surface of a Layered Half-Space. A Point Source at D=8km has a Step-like Pulse of 6-sec Length. Layer 1: v_{c1}=6km/sec, v_{s1}=4km/sec, ρ_1=3 gm/cm^3, 30km; Layer 2: v_{c2}=8km/sec, v_{s2}=1km/sec, ρ_2=4.5 gm/cm^3, 5km; Half-Space: v_{c3}=8km/sec, v_{s3}=4.5km/sec, ρ_3=4.5 gm/cm^3.

CONCLUSIONS

The finite-difference method for the solution of the wave equation is well adapted to the investigation of step-like displacement pulses from a point source in a layered half-space. A computation time of approximately 40 minutes is required for a displacement field of 11,500 grid points and 500 time cycles on a CDC 6400 computer. The computation time for a three-layer model is only slightly higher than that for the two-layer model for the same amount of grid points. Its exact value depends on the ratio of the number of horizontal to the number of vertical grid points in the displacement field. A displacement field of 11,500 points requires a memory capacity of 46,000 words to store the displacement arrays. The actual program requires 6,340 words in a CDC 6400 computer. Thus, the entire program length is 52,340 words. The investigation was carried out on a CDC 6400 with a 65,536-word central memory. The difference between central-memory size and program length is taken up by the computer system.

To investigate the permanent displacement on the surface of a layered half-space due to a step-like pulse of the displacement potential from a point source, the near-field term of the resulting displacement pulse may be used. It has the same time dependence as the potential pulse.

The total remnant displacement on the surface of a homogeneous isotropic half-space, caused by a step-like displacement pulse from a point source, is related to the distance from the source point as R^{-2}, as predicted by the theory of static elasticity. Minor discrepancies from this relationship apparent in dynamic calculations by the finite-difference method, are primarily due to the finite size of the region of elastic disturbance. In part, they are due to the inherent error in the finite-difference method.

For the two-layer model with a layer thickness of 4.375 source depths, $v_{c2}/v_{c1} = 4/3$, $v_{s2}/v_{s1} = 9/8$, and $\rho_2/\rho_1 = 3/2$, the total remnant displacement on the surface is related to the distance from the source point as $R^{-2.1}$ between the epicenter and 5 source depths epicentral distance. This relationship changes to $R^{-2.5}$ between epicentral distances of 7 and 8 source depths. As the shear-wave speed in the half-space of a two-layer model is decreased, leaving all other model parameters constant, the spatial attenuation for the remnant displacement decreases. For a model as described above, but with $v_{s2}/v_{s1} = 3/8$, the total remnant displacement on the surface is related to the distance from the source point as $R^{-1.8}$ between the 1 and 3 source depths epicentral distance. This relationship changes to $R^{-1.1}$ between epicentral distances of 7 and 8 source depths. The values for the last case are somewhat open to question

since the seismograms, on whose basis they were established, could not be carried far enough in time for the Rayleigh waves to die out. There is little doubt, however, that the attenuation of the remnant displacement on the surface of a layered half-space decreases, as the rigidity of the second layer decreases.

For the three-layer model, an increase of the remnant displacement on the surface is indicated, with decreasing rigidity of the second layer. This model induces a considerably more oscillatory band of Rayleigh-waves than the two-layer model. A quantitative evaluation of the remnant displacement was, therefore, not possible because it is masked by long-period Rayleigh waves within the length of the synthetic seismograms.

For the homogeneous isotropic half-space, the horizontal component of the remnant displacement on the surface arrives in two parts. At an epicentral distance of 8 source depths the remnant displacement is approximately 16 percent of its total amplitude after the arrival of the compressional-wave transient. The remaining 84 percent are added during the Rayleigh-wave transient.

For the layered half-space, the major contribution to the remnant displacement also arrives with the Rayleigh-wave train. The ratio of body wave to Rayleigh-wave contribution to the remnant displacement on the surface appears to depend on the rigidity of the second layer.

Use of a larger computer to carry the synthetic seismograms to greater length and the receiver positions to larger distances from the source will, without doubt, establish more concretely some of the relationships indicated in this research. The required storage of the computer increases approximately with the second power of the number of computed time cycles and with the second power of the number of space increments between the source and the receiver most distant from the source.

BIBLIOGRAPHY

Alterman, Z., Karal, F. C., Jr., 1968, Propagation of elastic waves in layered media by finite-difference methods: Seismol. Soc. America Bull., v. 58, no. 1, p. 367-398.

Alterman, Z., Karal, F. C., Jr., 1969, Errata, Seism, Soc. Am. Bull., v. 59, No. 1, p. 471.

Alterman, Z. S., and Kornfeld, P., 1968, Finite difference solution for pulse propagation in a sphere: Israel journ. of technology, v. 6, no. 1-2, p. 138-149.

Baranov, V., and Kunetz, G., 1960, Film synthetique avec reflexions multiples, theorie et calcul pratique: Geophysical Prospecting, v. 8, no. 2, p. 315-325.

Brian, P.L.T., 1961, A finite-difference method of high-order accuracy for solution of three-dimensional transient heat conduction problems: A.I.E. Ch. Journal, v. 7, no. 3, p. 367-370.

Cagniard, L., 1962, Reflection and refraction of progressive seismic waves, translated and revised by E. A. Flinn and C. H. Dix: McGraw-Hill Book Co., Inc.

Cherry, J. T., and Hurdlow, W. R., 1966, Numerical simulation of seismic disturbances: Geophysics, v. 31, no. 1, p. 33-49.

Collatz, L., 1966, Functional analysis on numerical mathematics: Oser. Academic Press, N.Y.

Davis, Ph. T., and Rabinowitz, Ph., 1967, Numerical Integration: Blaisdell Publishing Co., Waltham, Mass.

Ewing, W. M., Jardetzky, W. S., and Press, F., 1957, Elastic Waves in Layered media: McGraw-Hill Book Co., Inc.

Gutenberg, B., 1932: Handbuch der Geophysik. v. 4.

Hadsell, F. A., Major, M. W., 1967, Personal Communication.

Haskell, N. A., 1953, The dispersion of surface waves on multilayered media: Seismol. Soc. America Bull., v. 43, no. 1, p. 17-34.

Karal, F. C., Jr., 1968, Personal Communication.

Maenchen, G., and Sack, S., 1963, The Tensor Code: Lawrence Radiation Laboratory Report UCRL-7316.

Major, M. W., 1968, Personal Communication.

Sato, Y., 1959, Numerical Integration of the equation of motion for surface waves in a medium with arbitrary variation of material: Seismol. Soc. America Bull., v. 49, p. 57-77.

Wideman, C. T., Major, M. W., 1967, Strain steps associated with earthquakes: Seismol. Soc. America Bull., v. 57, no. 6, p. 1429-1444.